NINJ1 mediates plasma membrane rupture during lytic cell death

Nobuhiko Kayagaki (kayagaki.nobuhiko@gene.com)
Genentech, Inc.
Opher Kornfeld
Genentech, Inc.
Bettina Lee
Genentech
Irma Stowe
Genentech
Karen O'Rourke
Genentech, Inc.
Qingling Li
Genentech
Wendy Sandoval
Genentech Inc
Donghong Yan
Genentech, Inc
Min Xu
Genentech. Inc.
Gözde Ulas
Genentech. Inc.
Jian Payandeh
Genentech, Inc. https://orcid.org/0000-0002-4015-9716
Merone Roose-Girma
Genentech, Inc.
Zora Modrusan
Genentech, Inc.
Rohit Reja
Genentech
Meredith Sagolla
Genentech, Inc.
Joshua Webster
Genentech, Inc.
Vicky Cho

John Curtin School of Medical Research, ACT https://orcid.org/0000-0001-9039-9876

Thomas Andrews

Department of Immunology and Infectious Disease, John Curtin School of Medical Research, Australian National University

Lucy Morris

The Australian National University

Lisa Miosge

The Australian National University

Christopher Goodnow

Garvan Institute of Medical Research https://orcid.org/0000-0001-5296-6155

Edward Bertram

The Australian National University

Vishva Dixit

Genentech, Inc.

Research Article

Keywords: NINJ1, plasma membrane, lytic cell death

Posted Date: August 28th, 2020

DOI: https://doi.org/10.21203/rs.3.rs-62714/v1

Version of Record: A version of this preprint was published at Nature on January 20th, 2021. See the published version at https://doi.org/10.1038/s41586-021-03218-7.

NINJ1 mediates plasma membrane rupture during lytic cell death

Nobuhiko Kayagaki[1]*, Opher S. Kornfeld[1], Bettina L. Lee[1], Irma B. Stowe[1], Karen O'Rourke[1], Qingling Li[2], Wendy Sandoval[2], Donghong Yan[3], Min Xu[3], Gözde Ulas[4], Jian Payandeh[5], Merone Roose-Girma[6], Zora Modrusan[6], Rohit Reja[7], Meredith Sagolla[8], Joshua D. Webster[8], Vicky Cho[9,10], T. Daniel Andrews[10], Lucy X. Morris[9], Lisa A. Miosge[9,10], Christopher C. Goodnow[11], Edward M. Bertram[9,10], Vishva M. Dixit[1]*

[1]Department of Physiological Chemistry, [2]Department of Microchemistry, Proteomics and Lipidomics, [3]Department of Translational Immunology, [4]Department of Biochemical and Cellular Pharmacology, [5]Department of Structural Biology, [6]Department of Molecular Biology, [7]Department of Bioinformatics, and [8]Department of Pathology, Genentech Inc., South San Francisco, California, USA

[9]The Australian Phenomics Facility & [10]Department of Immunology and Infectious Diseases, The John Curtin School of Medical Research, The Australian National University, Canberra, ACT, Australia

[11]Garvan Institute of Medical Research, Sydney, NSW, Australia

*Co-corresponding Authors:

Nobuhiko Kayagaki, PhD
Genentech, Inc.
1 DNA Way
South San Francisco, CA 94080
Phone: (650)-225-2645
FAX: (650)-225-6443
e-mail: kayagaki@gene.com

Vishva M. Dixit, MD
Genentech, Inc.
1 DNA Way
South San Francisco, CA 94080
Phone: (650)-225-1312
FAX: (650)-225-6127
e-mail: dixit@gene.com

Abstract

Plasma membrane rupture (PMR) is the final cataclysmic event in lytic cell death. PMR releases intracellular molecules termed damage-associated molecular patterns (DAMPs) that propagate the inflammatory response. The underlying mechanism for PMR, however, is unknown. Here we show that the ill-characterized nerve injury-induced protein 1 (NINJ1) — a cell surface protein with two transmembrane regions — plays an essential role in the induction of PMR. A forward-genetic screen of randomly mutagenized mice linked NINJ1 to PMR. *Ninj1*$^{-/-}$ macrophages exhibited impaired PMR in response to diverse inducers of pyroptotic, necrotic and apoptotic cell death, and failed to release numerous intracellular proteins including High Mobility Group Box 1 (HMGB1, a known DAMP) and Lactate Dehydrogenase (LDH, a standard measure of PMR). *Ninj1*$^{-/-}$ macrophages died, but with a distinctive and persistent ballooned morphology, attributable to defective disintegration of bubble-like herniations. *Ninj1*$^{-/-}$ mice were more susceptible than wild-type mice to *Citrobacter rodentium*, suggesting a role for PMR in anti-bacterial host defense. Mechanistically, NINJ1 utilized an evolutionarily conserved extracellular α-helical domain for oligomerization and subsequent PMR. The discovery of NINJ1 as a mediator of PMR overturns the long-held dogma that cell death-related PMR is a passive event.

Pyroptosis is a potent inflammatory mode of lytic cell death triggered by diverse infectious and sterile insults[1-3]. It is driven by the pore-forming fragment of gasdermin D (GSDMD)[4-7] and releases two exemplar proteins: interleukin-1β (IL-1β), a pro-inflammatory cytokine, and LDH, a standard marker of PMR and lytic cell death. An early landmark study[8] predicted two sequential steps for pyroptosis: (1) initial formation of a small plasma membrane pore causing IL-1β release and non-selective ionic fluxes, and (2) subsequent PMR attributable to oncotic cell swelling. PMR releases LDH (140 kDa) and large DAMPs. While the predicted size of gasdermin pores (~18 nm inner diameter[9]) is large enough to release IL-1β (17 kDa, ~4.5 nm diameter), the underlying mechanism for subsequent PMR has been considered a passive osmotic lysis event.

An unbiased forward genetic screen identifies NINJ1

To identify essential mediators of PMR, we performed a forward genetic screen using bone marrow-derived macrophages (BMDMs) from N-ethyl-N-nitrosourea (ENU)-mutagenized mice. Cytoplasmic lipopolysaccharide (LPS), a potent stimulator of the non-canonical inflammasome,

was used to initiate caspase-11/GSDMD-dependent release of LDH[4,5] from BMDMs that were primed with the Toll-like Receptor 2 (TLR2) agonist Pam3CSK4. Pedigree IGL03767 exhibited a Mendelian-recessive trait that compromised LDH release (Fig. 1a). Exome sequencing of the founder G1 male identified 19 single nucleotide variants (SNVs). Subsequent phenotyping and SNV genotyping revealed that the trait correlated with inheritance of a point mutation in the gene encoding NINJ1 (Extended Data Fig. 1a, b, Extended Data Table1).

NINJ1 is a 16 kDa cell surface protein that has two transmembrane regions with N_{out}/C_{out} topology (Fig. 1b). NINJ1 is expressed ubiquitously, including in myeloid cells and the central nervous system, and reportedly functions as an adhesion molecule[10-12]. The SNV (a→t) occurred at the non-coding 3' splice acceptor site of exon 2 (Extended Data Fig. 1c). Accordingly, the 16 kDa NINJ1 protein detected in wild-type BMDMs was absent in *Ninj1*$^{mt/mt}$ BMDMs (Fig. 1c). *Ninj1*$^{mt/mt}$ BMDMs displayed attenuated GSDMD-dependent LDH release in response to either LPS or nigericin (an ionophore activator of the NLRP3 canonical inflammasome)[4,5,13] (Fig. 1d).

NINJ1 is essential for pyroptosis-related PMR

Like *Ninj1*$^{mt/mt}$ BMDMs, *Ninj1*$^{-/-}$ and *Gsdmd*$^{-/-}$ BMDMs released less LDH than wild-type BMDMs in response to LPS, nigericin, or infection with *Salmonella* Typhimurium, *Escherichia coli*, or *C. rodentium* (Fig. 2a, Extended Data Fig. 2a). We further assessed PMR by time-lapse live cell imaging of BMDMs preloaded with large dextran dyes (DD-150 or DD-70 kDa). LPS triggered less DD release from *Ninj1*$^{-/-}$ BMDMs than from wild-type BMDMs (Fig. 2b). Exogenous expression of NINJ1 in *Ninj1*$^{-/-}$ immortalized macrophages (iMACs) restored LPS-induced DD-150 release (Extended Data Fig. 2b), corroborating a critical role for NINJ1 in PMR. In contrast, NINJ1 deficiency did not impair the GSDMD-dependent release of a smaller dye (DD-3 kDa) or the intake of the 1.2 kDa cell-impermeable dye YOYO-1 (Fig. 2b). Thus, GSDMD pore formation appears intact in *Ninj1*$^{-/-}$ BMDMs. Consistent with this notion, wild-type and *Ninj1*$^{-/-}$ BMDMs both produced the N-terminal pore-forming fragment of GSDMD[4-7] in response to either nigericin or cytoplasmic LPS (Fig. 2c, Extended Data Fig. 2c). Collectively, these data reveal that NINJ1 is crucial for PMR, but dispensable for GSDMD pore formation.

IL-1β is a hallmark cytokine for pyroptosis that is thought to exit dying BMDMs through the GSDMD pore[1-3,8,9,14]. Accordingly, wild-type and *Ninj1*$^{-/-}$ BMDMs released comparable levels of IL-1β in response to either nigericin or cytoplasmic LPS (Fig. 2d). NINJ1 was also dispensable

for the release of IL-18, another pyroptosis-associated IL-1 family member (Extended Data Fig. 2d). Wild-type and *Ninj1*$^{-/-}$ BMDMs were mostly indistinguishable in transcriptomic analyses, lipid composition, and TLR-induced IL-6 and TNFα production (Extended Data Fig. 2e, f, g). In sum, our data provide compelling genetic evidence that the release of IL-1β and IL-18 from macrophages is independent of PMR and likely occurs via the ~18 nm GSDMD pore.

Wild-type BMDMs stimulated with either nigericin or cytoplasmic LPS undergo characteristic morphological changes during pyroptosis; they cease moving, swell, and develop bubble-like herniations that disintegrate abruptly to yield a shrunken corpse[2,8,15] (Fig. 2e, f, Supplementary Video 1, 2). NINJ1 deficiency inhibited bubble disintegration while upstream events were unaltered. Remarkably, even 16 h post LPS or nigericin exposure, *Ninj1*$^{-/-}$ BMDMs retained prominent "bubble" morphology (Fig. 2e). The cells were dead based on their loss of ATP, mitochondrial membrane potential (MMP), and motility (Fig. 2g, Extended Data Fig. 2h, Supplementary Video 1, 2). Thus, PMR and related events, including LDH release and bubble disintegration, are genetically separable from GSDMD-driven cell death and IL-1β release. PMR is likely a post-cell death event[15,16]. Of note, BMDMs ceased moving prior to bubble formation (Supplementary Video 1, 2). NINJ1-independent loss of MMP also preceded PMR (as assessed by DD-150 release, Extended Data Fig. 2h, i).

We confirmed that NINJ1-mediated PMR released more proteins than just LDH. Supernatants from wild-type BMDMs stimulated with nigericin or cytoplasmic LPS contained many proteins that were diminished in their *Ninj1*$^{-/-}$ counterparts (Fig. 2h, Extended Data Fig. 2j). Subsequent secretome analysis detected ~780 molecules (including Plectin) that were released in a NINJ1-dependent manner in response to cytoplasmic LPS (Fig. 2i, Extended Data Table2). Of note, *Ninj1*$^{-/-}$ BMDMs failed to release High Mobility Group Box 1 (HMGB1), a proinflammatory DAMP[17], despite exhibiting normal GSDMD-dependent release of IL-1α (Fig. 2j, k). HMGB1 is a relatively small ~28 kDa nuclear protein, but can form large complexes with nucleosomes and transcription factors[18], which likely hinders its release through the ~18 nm GSDMD pore. Regardless, the NINJ1-dependent release of diverse intracellular proteins from pyroptotic cells, including HMGB1, suggests a pro-inflammatory role of NINJ1. Indeed, *Ninj1*$^{-/-}$ mice were more susceptible than wild-type mice to infection with *C. rodentium* (Fig. 2l). Thus, NINJ1-dependent PMR may release DAMPs that are important for host defense against bacteria.

NINJ1 plays a global role in PMR induction

PMR is not exclusive to pyroptosis, also occurring during necrosis or post-apoptosis (sometimes referred to as secondary necrosis)[19]. We examined the role of NINJ1 in non-pyroptotic PMR. In control experiments, pyroptotic stimuli (cytoplasmic LPS, nigericin, and flagellin[3,4]) caused NINJ1- and GSDMD-dependent PMR in BMDMs based on LDH release, whereas PMR following freezing and thawing of cells did not require NINJ1. (Fig. 3a). *Ninj1*$^{-/-}$ BMDMs released less LDH than wild-type BMDMs in response to necrotic stimuli (bacterial pore-forming toxins) or apoptotic stimuli (including chemotherapeutics such as cisplatin (DNA-crosslinker) and venetoclax (BCL2-antagonist))[20]. The release of HMGB1 and other proteins from BMDMs in response to cisplatin or venetoclax was also attenuated by NINJ1 deficiency (Fig. 3b, Extended Data Fig. 3a). Wild-type BMDMs treated with venetoclax exhibited typical apoptotic morphology[21] including cell shrinkage and bleb formation. Blebbing was not prevented by *Ninj1* deficiency but the dying cells developed a persistent ballooned morphology (Fig. 3c, d, Extended Data Fig. 3b, Supplementary Video 3). These data underscore a global role for NINJ1 in inducing PMR.

We confirmed that venetoclax-induced PMR in BMDMs was a gasdermin-independent, non-pyroptotic event. BMDMs express only *Gsdmd* and *Gsdme*[22,23] (Extended Data Fig. 3c), but *Gsdmd*$^{-/-}$*Gsdme*$^{-/-}$ BMDMs exhibited normal PMR in response to venetoclax, releasing both DD-150 and LDH (Fig. 3e, f). Mitochondrial dysfunction, which causes ATP depletion and consequent cell swelling[20,24], may be responsible for apoptosis-related PMR. Indeed, oligomycin (an inhibitor of ATP synthase), like venetoclax, induced gasdermin-independent but NINJ1-dependent PMR (Fig. 3f, g, h, Extended Data Fig. 3d, e).

NINJ1 is unlikely to be the only mediator of PMR because NINJ1 deficiency only partially attenuated the release of LDH and DD-150 from BMDMs induced to undergo mixed lineage kinase domain-like (MLKL)-dependent necroptosis[25,26] by treating with TNF plus the pan-caspase inhibitor zVAD (Fig. 3i, j). Furthermore, overall protein release, including the release of HMGB1, was largely unaltered (Extended Data Fig. 3f, g). These data support the existence of a NINJ1-independent mechanism for PMR during necroptosis. It is possible that oligomerized MLKL[26] disrupts the plasma membrane to induce PMR directly, thereby bypassing the need for NINJ1.

NINJ1 oligomerizes for induction of PMR

Ectopic expression of NINJ1 (human or mouse) in HEK293T cells caused marked cytotoxicity with LDH release (Fig. 4a, Extended Data Fig. 4a, b). *Drosophila* orthologs dNINJ-A and -B were also cytotoxic, whereas dNINJ-C and NINJ2 were not (Fig. 4a, Extended Data Fig. 4c). Scanning mutagenesis identified the highly conserved extracellular α-helical domain as crucial for cell killing (Fig. 4b, Extended Data Fig. 4d, e). All NINJ1 mutants that harbored five consecutive alanine substitutions within the α-helical domain (including A_{42}NKKS→A_{42}AAAA) exhibited impaired cytotoxic activity. Mutating a residue within the α-helix domain to a helix-breaking proline (including A_{59}P), also reduced NINJ1 killing activity (Extended Data Fig. 5a), confirming the importance of this conserved α-helix structure.

NINJ1 reportedly functions as a cell-cell adhesion molecule via homotypic binding of an adhesive segment (26-37aa)[10,11] prior to the α-helix domain. However, mutagenesis of this evolutionarily variable segment did not reduce NINJ1 killing activity (Fig. 4b, Extended Data Fig. 4e). The previously reported adhesion-dead NINJ1 (W_{29}A)[11] also restored LPS-induced PMR in *Ninj1*$^{-/-}$ iMACs (Extended Data Fig. 5b). Thus, the adhesive segment of NINJ1 appears dispensable for PMR.

We investigated NINJ1 activation in BMDMs using standard biochemical approaches. By SDS-PAGE, with or without reductant (DTT), NINJ1 migrated as a ~16 kDa monomer regardless of stimulus (LPS, nigericin, TLRs, or interferons) or treatment with the pan-kinase inhibitor staurosporine (Extended Data Fig. 5c, d, e). By blue native PAGE (BN-PAGE), which maintains native structures, NINJ1 shifted from ~40 kDa to ~900 kDa in response to nigericin or cytoplasmic LPS (Fig. 4c). These data suggest that NINJ1 exists as a dimer or trimer in unstimulated BMDMs, and then oligomerizes in response to death stimuli. By immunofluorescence microscopy of unstimulated BMDMs, NINJ1 primarily localized at the plasma membrane alongside the surface marker CD44, although some NINJ1, probably in transit, was co-stained with Golgi marker GM130 (Extended Data Fig. 6). Upon nigericin stimulation, NINJ1 formed multiple speck-like assemblies (Fig. 4d), consistent with NINJ1 oligomerization.

The NINJ1 extracellular α-helix domain possesses characteristic hydrophilic and hydrophobic clusters reminiscent of amphipathic α-helices[27,28] (Extended Data Fig. 7a). Of note, amphipathic α-helix-containing proteins like α-Synuclein disrupt phospholipid bilayer membranes by an ill-defined mechanism where positively charged residues play critical roles[29,30]. Mutagenesis of positively charged α-helix residues (H_{40}, K_{44}, K_{45}, K_{65}) to glutamine (a non-charged aa)

uncovered a $K_{45}Q$ mutation that impaired NINJ1 cytotoxicity in HEK293T cells (Fig. 4e, Extended Data Fig. 7b). The K_{45} residue is evolutionarily conserved and predicted to be near the N-terminal side of the α-helix (Extended Data Fig. 4e, 7a). Both NINJ1 $K_{45}Q$ and $A_{59}P$ failed to restore LPS-induced PMR in *Ninj1*$^{-/-}$ iMACs, and attenuated oligomerization of NINJ1 (Fig. 4f, g). These data support a model in which NINJ1 oligomerizes to induce PMR. Precisely how NINJ1 induces PMR remains unclear and will likely require further structural insights.

In summary, NINJ1 is an evolutionarily conserved cell surface protein that mediates PMR and DAMP release, which are key events in the propagation of inflammation. Given the potent and global role for NINJ1 in PMR induction and DAMP-release related to pyroptosis, apoptosis, and necrosis, targeting NINJ1 may therapeutically benefit patients with cell death-driven inflammation.

Acknowledgements

We thank the staff of the Australian Phenomics Facility, Genentech Transgenic Technology, imaging cores, and antibody engineering group, Shuang Wu, Sarah Gierke, Fermin Gallardo-Chang, and Wayne Fairbrother for technical expertise and discussion, Kim Newton for manuscript editing, and W. Alexander for *Mlkl*$^{-/-}$ mice. Fig. 2b was created with biorender.com.

Author contributions

N.K., O.S.K., B.L.L., I.B.S., K.O., G.U., J.P., Z.M., M.S. V.C., T.D.A, L.X.M. and L.A.M. designed and performed experiments, Q.L. and W.S. performed secretome and lipidomics analysis, D.Y. and M.X. performed *in vivo* study, M.R.-G. generated the *Ninj1*$^{-/-}$ mice, O.S.K. and R.R. provided computational analysis and C.C.G., E.M.B., and V.M.D. contributed to experimental design. N.K. wrote the paper with input from all authors.

Author information

Reprints and permissions information is available at www.nature.com/reprints. Most authors were employees of Genentech, Inc. Correspondence and requests for materials should be addressed to kayagaki@gene.com or dixit@gene.com.

Data availability

RNA-sequencing data wil be available through the GEO database. Source Data for Figs. 1–4 and Extended Data Figs. 2–5 are provided with the paper. Other datasets generated during and/or analysed during the current study are available from the corresponding authors on reasonable request.

Figure Legends

Figure 1 | Forward genetic screen identifies a mutation in *Ninj1* that abolishes plasma membrane rupture (PMR)

a, Screening of third-generation (G3) offspring from ENU-treated C57BL/6 mice. Graph shows LDH released from Pam3CSK4 (TLR2 agonist)-primed bone marrow-derived macrophages (BMDMs) after LPS electroporation. Red dot represents IGL03767 G3 7 (Extended Data Fig. 1a, b). Grey dots represent other G3 mice in the same batch from multiple pedigrees. Black, *Caspase-11*$^{mt/mt}$ 129X1/SvJ mouse.

b, Predicted structure of NINJ1. Blue, extracellular α-helix domain. EXT, extracellular region. TM, transmembrane domain. CYT, cytoplasmic region.

c, Immunoblot of NINJ1 from BMDM extracts. Lane numbers indicate different mice. *n*=2 per genotype. Wt, wild-type.

d, LDH released from primed BMDMs stimulated with LPS electroporation or nigericin. Cont, medium alone. Data are means (bars) of at least three individual replicates (circles). *n*=2 per genotype.

Figure 2 | NINJ1 is essential for pyroptosis-related PMR

a, LDH released from primed BMDMs stimulated by LPS electroporation, nigericin or indicated bacteria, or treated with 0.25 % triton.

b, Release of indicated kDa sizes of dextran dye (DD) or LDH, or incorporation of YOYO-1 in live cell imaging analysis with primed BMDMs following LPS electroporation over a 16 h time course. Data are means (circles) ± SD (shaded area) of three individual replicates.

c, Immunoblot of GSDMD, GSDMD-N-terminal fragment (GSDMD-NT), and NINJ1 in supernatant + extract from primed BMDMs after stimulation with LPS electroporation.

d, Release of IL-1β from primed BMDMs stimulated with LPS electroporation or nigericin.

e, Bright-field images of primed BMDMs stimulated with LPS transfection or nigericin for 16 h.

f, Single cell time course images of primed BMDMs following LPS transfection.

g, Viability (top) or LDH release (bottom) of primed BMDMs at 16 h after LPS electroporation.

h, i, Silver staining (**h**) or volcano plot (**i**) of released proteins in culture supernatant of LPS electroporation-stimulated primed BMDMs. FC, fold change.

j, Release of HMGB1 or IL-1α from BMDMs as **d.**

k, Model for pyroptosis-related PMR

l, Kaplan–Meier survival plots for mice infected with *Citrobacter rodentium. P* value was calculated by a two-sided Gehan–Breslow–Wilcoxon test.

Figure 3 | NINJ1 plays a global role in PMR induction

a, LDH released from BMDMs after freeze/thaw cycle or culture with inducers of pyroptosis (LPS, nigericin, flagellin), necrosis (pore-forming toxins (listeriolysin O (LSO) and streptolysin O (SLO)), or apoptosis (venetoclax, doxorubicin, cisplatin and FasL).

b, Silver stain of culture supernatant from venetoclax-stimulated BMDMs.

c, Bright-field images of BMDMs cultured with venetoclax.

d, Single cell time lapse images of BMDMs cultured with venetoclax.

e, **g**, **j**, Release of DD-150 in BMDMs live cell imaging analysis following treatment with venetoclax (**e**), oligomycin (**g**), or TNF+zVAD (**j**).

f, **i,** LDH release from BMDMs stimulated with venetoclax, oligomycin (**f**), or TNF+zVAD (**i**).

h, Model for apoptosis-related PMR.

Figure 4 | NINJ1 oligomerizes for induction of PMR

a, Cytotoxicity of human and mouse NINJ1, NINJ2, and fly NINJ (dNINJ-A, B, C) in HEK293T cells.

b, NINJ1 domain structure (top). Conservation of NINJ1 amino acid (aa) residues as scored by ConSurf profile (middle). Cytotoxicity of wild-type and 5-Ala scan NINJ1 mutants in HEK293T cells (bottom). Numbers indicate aa positions replaced by 5-Ala. Killing score is cytotoxicity normalized against wild-type NINJ1 control.

c, Blue Native (BN)-PAGE analysis of NINJ1 in primed BMDMs following LPS or nigericin stimulation for indicated periods.

d, Immunofluorescence microscopy of NINJ1 in nigericin-stimulated primed BMDMs.

e, Cytotoxicity of NINJ1 mutants in HEK293T cells.

f, DD-150 dye release from *Ninj1*$^{-/-}$ iMACs reconstituted with NINJ1 following LPS electroporation.

g, BN-PAGE analysis of NINJ1 in LPS electroporation-stimulated iMACs.

Extended Data Figure 1 | Homozygosity of the *Ninj1* point mutation correlates with low responsiveness to LPS

a, *Ninj1* genotypes and screen phenotypes of mice derived from IGL03767. Identification numbers of screened animals are shown. G, generation.

b, Nineteen SNV genotypes mutated in the pedigree and their phenotypes.

c, Wild-type and IGL03767 *Ninj1* genes. exon 2 coding sequence is in uppercase and SNV mutation is in bold and highlighted with an asterisk. Grey boxes represent exons.

Extended Data Figure 2 | NINJ1 is essential for pyroptosis-related PMR

a, Immunoblot of NINJ1 and GSDMD in BMDM lysates.

b, Release of DD-150 in live cell imaging analysis of iMACs following LPS electroporation over a 16 h time course (left). Immunoblot of NINJ1 in *Ninj1*$^{-/-}$ iMACs reconstituted with NINJ1 (right).

c, Immunoblot of GSDMD, GSDMD-N-terminal fragment (NT), and NINJ1 in supernatant + extract from nigericin-stimulated primed BMDMs.

d, LDH or IL-18 release from BMDMs stimulated as Fig. 2d

e, IL-6 or TNFα production from BMDMs stimulated with Pam3CSK4 (TLR2) or extracellular LPS (TLR4).

f, Lipid composition of primed BMDMs. Lipids profiled are diacylglycerol (DAG), dihydroceramide (DCER), hexosylceramide (HCER), lactosylceramide (LCER), lysophosphatidylcholine (LPC), lysophosphatidylethanolamine (LPE), phosphatidylcholine (PC), phosphatidylethanolamine (PE), sphingomyelin (SM), triacylglycerol (TAG), cholesteryl ester (CE), and ceramide (CER).

g, RNA-seq of primed BMDMs.

h, Time-lapse imaging analysis of mitochondrial membrane potential (MMP) as measured by tetramethylrhodamine methyl ester perchlorate (TMRM) in primed BMDMs following LPS electroporation.

i, Single cell time-lapse imaging analysis of TMRM and DD-150 release in primed wild-type BMDMs following LPS electroporation. Timepoint 0 corresponds to the point of maximal TMRM decline for each cell.

j, Silver staining of proteins in culture supernatant of nigericin-stimulated primed BMDMs.

Extended Data Figure 3 | NINJ1 plays a global role in PMR induction related to pyroptosis, apoptosis, and necrosis

a, d, g, Release of HMGB1 from BMDMs stimulated with cisplatin, venetoclax, oligomycin (**a**, **d**), or TNF+zVAD (**g**).

b, Viability (left) or LDH release (right) of venetoclax-stimulated BMDMs.

c, Expression of indicated gasdermin transcripts in RNA-seq analysis of BMDMs. FPKM, fragments per kilobase of transcript per million mapped reads.

e, Bright-field images of BMDMs cultured with oligomycin.

f, Silver staining of proteins in culture supernatant of TNF+zVAD-stimulated BMDMs.

Extended Data Figure 4 | Conservation of NINJ1 throughout evolution

a, d, Immunoblot of FLAG NINJ1 from Fig. 4a (**a**) or b (**d**).

b, LDH release from transfected 293T cells.

c, Phylogenetic tree of NINJ1 and NINJ2. Numbers represent standardized distance scores (number of amino acid substitutions per length of the alignment).

e, Multiple alignment of NINJ1 aa sequences with the extracellular alpha helix domain predicted by JPred highlighted in blue. TM, transmembrane domain.

Extended Data Figure 5 | Biochemical analysis of NINJ1

a, NINJ1 domain structure (top). Cytotoxicity of wild-type NINJ1 or NINJ1 with proline point mutants in HEK293Ts (middle). Numbers indicate aa positions where residues were replaced by Proline. Cytotoxicity was normalized against wild-type NINJ1 control. Immunoblot of FLAG-NINJ1 (bottom). Killing score is cytotoxicity normalized against wild-type NINJ1 control.

b. Release of DD-150 in live cell imaging of *Ninj1*$^{-/-}$ iMACs reconstituted with NINJ1 following LPS electroporation (left). Immunoblot of iMACs with anti-NINJ1 polyclonal Ab (right).

c, d, Immunoblot of NINJ1 in primed BMDMDs stimulated with LPS electroporation or nigericin (**c**), or in non-primed BMDMDs cultured with indicated stimuli (**d**).

e, Phos-tag SDS-PAGE analysis of LPS electroporation- or nigericin-stimulated primed BMDMs with or without staurosporine pretreatment. S6, ribosomal protein S6.

Extended Data Figure 6 | Subcellular localization of NINJ1

Immunofluorescence microscopy of NINJ1 and indicated markers in primed BMDM.

Extended Data Figure 7 | Computational model of NINJ1 extracellular α-helix domain

a, Computational model of NINJ1 extracellular α-helix domain. Grey, hydrophobic residues. Blue, negatively charged residues. Light blue, polar residues. Red, positively charged residues.

b, Immunoblot of FLAG-NINJ1 in HEK293T cells from Fig. 4e.

Extended Data Figure 8 | Characterization of *Gsdmd*$^{-/-}$*Gsdme*$^{-/-}$ BMDMs and anti-NINJ1 monoclonal Ab.

a, Immunoblot of GSDME in BMDMs.

b, Immunoblot with anti-NINJ1 monoclonal Ab clone 25 in HEK293T cells transfected with indicated FLAG-tagged constructs.

Extended Data Table 1 | Bioinformatic analysis of ENU-induced SNVs present in IGL03767 pedigree

Extended Data Table 2 | List of top hits from secretome analysis (Fig. 2i).

Supplementary Video 1 | *Ninj1*$^{-/-}$ BMDMs die with persistent ballooned morphology in response to nigericin.

Time-lapse imaging of primed BMDMs following nigericin stimulation (every 5 minutes for a total of 800 minutes).

Supplementary Video 2 | *Ninj1*$^{-/-}$ BMDMs die with persistent ballooned morphology in response to LPS.

Time-lapse imaging of primed BMDMs following LPS transfection (every 5 minutes for a total of 800 minutes).

Supplementary Video 3 | Venetoclax-stimulated *Ninj1*$^{-/-}$ BMDMs retain prominent bubble morphology

Time-lapse imaging of venetoclax-stimulated BMDMs (every 3 minutes after 290 minutes of stimulation for 430 minutes).

References

1 Cookson, B. T. & Brennan, M. A. Pro-inflammatory programmed cell death. *Trends Microbiol* **9**, 113-114 (2001).

2 Gaidt, M. M. & Hornung, V. Pore formation by GSDMD is the effector mechanism of pyroptosis. *Embo J* **35**, 2167-2169, doi:10.15252/embj.201695415 (2016).

3 Kayagaki, N. & Dixit, V. M. Rescue from a fiery death: A therapeutic endeavor. *Science* **366**, 688-689, doi:10.1126/science.aaw1177 (2019).

4 Shi, J. *et al.* Cleavage of GSDMD by inflammatory caspases determines pyroptotic cell death. *Nature* **526**, 660-665, doi:10.1038/nature15514 (2015).

5 Kayagaki, N. *et al.* Caspase-11 cleaves gasdermin D for non-canonical inflammasome signalling. *Nature* **526**, 666-671, doi:10.1038/nature15541 (2015).

6 Ding, J. *et al.* Pore-forming activity and structural autoinhibition of the gasdermin family. *Nature* **535**, 111-116, doi:10.1038/nature18590 (2016).

7 Liu, X. *et al.* Inflammasome-activated gasdermin D causes pyroptosis by forming membrane pores. *Nature* **535**, 153-158, doi:10.1038/nature18629 (2016).

8 Fink, S. L. & Cookson, B. T. Caspase-1-dependent pore formation during pyroptosis leads to osmotic lysis of infected host macrophages. *Cellular microbiology* **8**, 1812-1825, doi:10.1111/j.1462-5822.2006.00751.x (2006).

9 Ruan, J., Xia, S., Liu, X., Lieberman, J. & Wu, H. Cryo-EM structure of the gasdermin A3 membrane pore. *Nature* **557**, 62-67, doi:10.1038/s41586-018-0058-6 (2018).

10 Araki, T. & Milbrandt, J. Ninjurin, a novel adhesion molecule, is induced by nerve injury and promotes axonal growth. *Neuron* **17**, 353-361, doi:10.1016/s0896-6273(00)80166-x (1996).

11 Araki, T., Zimonjic, D. B., Popescu, N. C. & Milbrandt, J. Mechanism of homophilic binding mediated by ninjurin, a novel widely expressed adhesion molecule. *J Biol Chem* **272**, 21373-21380, doi:10.1074/jbc.272.34.21373 (1997).

12 Ahn, B. J. *et al.* Ninjurin1 is expressed in myeloid cells and mediates endothelium adhesion in the brains of EAE rats. *Biochem Biophys Res Commun* **387**, 321-325, doi:10.1016/j.bbrc.2009.07.019 (2009).

13 Kayagaki, N. *et al.* Non-canonical inflammasome activation targets caspase-11. *Nature* **479**, 117-121, doi:10.1038/nature10558 (2011).

14 Liu, T. *et al.* Single-cell imaging of caspase-1 dynamics reveals an all-or-none inflammasome signaling response. *Cell reports* **8**, 974-982, doi:10.1016/j.celrep.2014.07.012 (2014).

15 de Vasconcelos, N. M., Van Opdenbosch, N., Van Gorp, H., Parthoens, E. & Lamkanfi, M. Single-cell analysis of pyroptosis dynamics reveals conserved GSDMD-mediated subcellular events that precede plasma membrane rupture. *Cell Death Differ* **26**, 146-161, doi:10.1038/s41418-018-0106-7 (2019).

16 DiPeso, L., Ji, D. X., Vance, R. E. & Price, J. V. Cell death and cell lysis are separable events during pyroptosis. *Cell Death Discov* **3**, 17070, doi:10.1038/cddiscovery.2017.70 (2017).

17 Andersson, U. & Tracey, K. J. HMGB1 is a therapeutic target for sterile inflammation and infection. *Annu Rev Immunol* **29**, 139-162, doi:10.1146/annurev-immunol-030409-101323 (2011).

18 Stros, M. HMGB proteins: interactions with DNA and chromatin. *Biochimica et biophysica acta* **1799**, 101-113, doi:10.1016/j.bbagrm.2009.09.008 (2010).
19 Silva, M. T. Secondary necrosis: the natural outcome of the complete apoptotic program. *FEBS Lett* **584**, 4491-4499, doi:10.1016/j.febslet.2010.10.046 (2010).
20 Ashkenazi, A., Fairbrother, W. J., Leverson, J. D. & Souers, A. J. From basic apoptosis discoveries to advanced selective BCL-2 family inhibitors. *Nature reviews. Drug discovery* **16**, 273-284, doi:10.1038/nrd.2016.253 (2017).
21 Kerr, J. F., Wyllie, A. H. & Currie, A. R. Apoptosis: a basic biological phenomenon with wide-ranging implications in tissue kinetics. *Br J Cancer* **26**, 239-257, doi:10.1038/bjc.1972.33 (1972).
22 Rogers, C. *et al.* Cleavage of DFNA5 by caspase-3 during apoptosis mediates progression to secondary necrotic/pyroptotic cell death. *Nature communications* **8**, 14128, doi:10.1038/ncomms14128 (2017).
23 Wang, Y. *et al.* Chemotherapy drugs induce pyroptosis through caspase-3 cleavage of a gasdermin. *Nature* **547**, 99-103, doi:10.1038/nature22393 (2017).
24 Dijkstra, K., Hofmeijer, J., van Gils, S. A. & van Putten, M. J. A Biophysical Model for Cytotoxic Cell Swelling. *J Neurosci* **36**, 11881-11890, doi:10.1523/JNEUROSCI.1934-16.2016 (2016).
25 Sun, L. *et al.* Mixed lineage kinase domain-like protein mediates necrosis signaling downstream of RIP3 kinase. *Cell* **148**, 213-227, doi:10.1016/j.cell.2011.11.031 (2012).
26 Grootjans, S., Vanden Berghe, T. & Vandenabeele, P. Initiation and execution mechanisms of necroptosis: an overview. *Cell Death Differ* **24**, 1184-1195, doi:10.1038/cdd.2017.65 (2017).
27 Drin, G. & Antonny, B. Amphipathic helices and membrane curvature. *FEBS Lett* **584**, 1840-1847, doi:10.1016/j.febslet.2009.10.022 (2010).
28 Peter, B. J. *et al.* BAR domains as sensors of membrane curvature: the amphiphysin BAR structure. *Science* **303**, 495-499, doi:10.1126/science.1092586 (2004).
29 Auluck, P. K., Caraveo, G. & Lindquist, S. alpha-Synuclein: membrane interactions and toxicity in Parkinson's disease. *Annu Rev Cell Dev Biol* **26**, 211-233, doi:10.1146/annurev.cellbio.042308.113313 (2010).
30 Zasloff, M. Antimicrobial peptides of multicellular organisms. *Nature* **415**, 389-395, doi:10.1038/415389a (2002).

Materials and Methods

ENU-mutagenized mouse strains

C57BL/6NCrl generation (G) 0 mice were treated with ethylnitrosourea (ENU) and the resulting mutations were bred to homozygosity in G3 mice as previously described[31]. All animals used in this study were cared for and used in experiments approved by the Australian National University Animal Experimentation Ethics Committee under protocol A2018/07. 129X1/SvJ strain was used as a *Casp11* mutant[13] control.

Exome sequencing

Exon capture, sequencing and analysis were performed as previously described[32,33]. *Ninj1* mutant genotyping primer sequences:
F1: GAAGGTGACCAAGTTCATGCTCTGACCGCCTTGCTCCCACA,
F2: GAAGGTCGGAGTCAACGGATTCTGACCGCCTTGCTCCCACT,
R1: CGCTCTTCTTGTTGGCATAA.

Other mice

Gsdmd$^{-/-}$ (1,632 bp deletion[5]) and *Mlkl*$^{-/-}$mice[34] with C57BL/6N background were described previously. *Gsdme*$^{-/-}$ (2 bp deletion at exon 3) mice with C57BL/6N background were genotyped with PCR primers (5′- TACCTCTTGACGGCATCC and 5′- ATACGAGAGCAAGTGTGAGA) yielding a 171 bp wild-type DNA fragment and a 169 bp mutant DNA fragment, and crossed with *Gsdmd*$^{-/-}$ mice to generate *Gsdmd*$^{-/-}$*Gsdme*$^{-/-}$ mice (Extended Data Fig. 8a). *Ninj1*$^{-/-}$ mice were obtained by electroporation-based strategy of C57BL/6N zygotes with 25 ng/μl wild-type Cas9 mRNA (Thermo Fisher Scientific) and 13 ng/μl *in vitro*-transcribed 2 single-guide RNAs into mouse zygotes[35]. Tail DNA from resulting offspring was analyzed by PCR and sequencing. Target sequences of sgRNA used to knockout exon 2 are: 5′-AAGGTGACCAACGTCCTGTA-3’ PAM: GGG with an CFD algorithm score of 97, and the 5′-CCATACGCCTTACTCCCTGA-3’PAM:GGG with an CFD algorithm score of 94. The 867 bp knockout region corresponds to GRCm38/mm10 chr13: 49,193,197- 49,194,063. *Ninj1*$^{-/-}$ mice were genotyped with PCR primers (FAM 5′-CAGGTTGGTGGTACATCTATTG, 5′-GCAGCAGGTACTTCTCC, and 5′-ACGGACGACCAGTGATTA) yielding a 358 bp wild-type DNA fragment and a 408 bp mutant

DNA fragment. For wild-type control, *Ninj1*$^{+/+}$ littermate mice were used. All animal procedures were conducted under protocols approved by the Genentech Institutional Animal Care and Use Committee in an Association for Assessment and Accreditation of Laboratory Animal Care (AAALAC)-accredited facility in accordance with the Guide for the Care and Use of Laboratory Animals and applicable laws and regulations.

Reagents and antibodies

Ultra-pure LPS (E. coli O111:B4, InvivoGen), Pam3CSK4 (InvivoGen), IFN-α, (PBL Assay Science), IFN-γ (eBioscience), nigericin (MilliporeSigma), Ultra-pure flagellin (from *P. aeruginosa*, InvivoGen), cholera toxin B (CTB, List Biological Labs), venetoclax (TOCRIS), doxorubicin (Enzo Life Sciences), cisplatin (Fresenius Kabi), oligomycin A (TOCRIS), staurosporine (Enzo Life Sciences), TNFα (in-house Genentech), carbobenzoxy-valyl-alanyl-aspartyl-[O-methyl]-fluoromethylketone (z-VAD-FMK, Promega), Listeriolysin-O (LLO, US Biologicals), Streptolysin-O (SLO, US Biologicals) and FasL (MegaFasL, AdipoGen). Antibodies used include: GSDMD (clone 17G2G9[36], Genentech), cleaved GSDMD (50928S, Cell Signaling Technology), GSDME polyclonal Ab (raised against mouse GSDME E_{74}-G_{93} peptide, rabbit IgG, Genentech, Extended Data Fig. 8a), S6 ribosomal protein (5G10, Cell Signaling Technology), Phospho-S6 (D57.2.2E, Cell Signaling Technology), β-actin HRP (AC-15, Novus Biologicals), FLAG epitope (M2 HRP, MilliporeSigma), and NINJ1 monoclonal Ab (raised against mouse NINJ1 extracellular domain 1, epitope P_{22}-L_{31}, rabbit IgG2b, clone 25, Genentech, Extended Data Fig. 8b). Where indicated, NINJ1 polyclonal Ab (raised against mouse NINJ1 extracellular domain 1, rabbit IgG, Genentech) was used.

BMDM stimulation

Bone marrow cells were differentiated into macrophages in Dulbecco's modified Eagle's medium (DMEM) supplemented with 10 % (v/v) low-endotoxin fetal bovine serum (FBS; Omega Scientific) and 20 % (v/v) L929-conditioned medium at 37 ℃ with 5 % CO_2 and were harvested on day 5 for experiments. For stimulation, cells were plated overnight at ~1.0×10^6 cells/ml in 100 µl on 96-well plates or in 500 µl for 24-well plates. For 96-well–based inflammasome stimulations, cells were primed with Pam3CSK4 (1 µg/ml) for 5 hours where indicated, which was followed by stimulation with 10 µg/ml nigericin, or LPS (described as follows) in Opti-MEM I media (Thermo

Fisher Scientific). For intracellular LPS electroporation[37], primed BMDMs were electroporated with the Amaxa 4D Nucleofector Y Unit (Lonza) in Opti-MEM I medium with LPS (5 μg/ml) in 24-well plates. Unless indicated, after 1 h nigericin or 2 h LPS electroporation, cells and culture supernatant were subjected to analysis. For flagellin stimulation, primed BMDMs were electroporated with flagellin (0.5 μg/ml) with AMAXA 4D and cultured for 0.5 h. For bacterial infections with *E. coli* (ATCC 11775, MOI 30), *C. rodentium* (ATCC 51116, MOI 20) *and S.* Typhimurium (SL1344, MOI 10), primed BMDMs were cultured with bacteria for 1.5 h and then gentamicin (Thermo Fisher Scientific) was added to cultures at 100 μg/ml, which was followed by additional incubation for a total 16 h. For FasL (0.5 μg/ml for 6 h), oligomycin (12.6 μM for 16 h), venetoclax (25 μM for 16 h), doxorubicin (10 μM for 16 h), cisplatin (10 μg/ml for 16 h), LLO (2 μg /ml for 6 h), SLO (1 μg/ml for 6 h), TNF+zVAD (TNFα 100 ng/ml + z-VAD-FMK 20 μM for 16 h), non-primed BMDMs were used. For triton lysis controls, cells were lysed with 0.25 % triton-x in corresponding media. For freeze and thaw, cells were frozen at -80 °C for 30 min in 96-well plates, then thawed at room temperature. For TLR or interferon stimulation, BMDMs were cultured with Pam3CSK4 (1 μg/ml), LPS (1 μg/ml), IFN-α (100 ng/ml) and IFN-γ (100 ng/ml) and stimulated for 6 h. For staurosporine treatment, primed BMDM were pre-cultured with 1 μM staurosporine for 30 min prior to LPS or nigericin stimulation.

Cell assays and cytokine measurements

Culture medium was analyzed for LDH release with the CytoTox 96 Non-Radioactive Cytotoxicity Assay (Promega), IL-1β secretion with the Mouse IL-1β Tissue Culture Kit (Meso Scale Discovery). Enzyme-linked immunosorbent assay kits were used to assay IL-18 (MBL International), IL-1α (Thermo Fisher Scientific), and HMGB1 (IBL). For IL-6 and TNFα, Luminex analysis was run with Milliplex Mouse Panel I 32-plex (MilliporeSigma). CellTiter-Glo reagent (Promega) was used for ATP assay for detection of viable cells. For YOYO-1 staining, media containing YOYO-1 (491/509) dye (Thermo Fisher Scientific) at a final concentration of 200 nM was added at the time of stimulation. Images were scanned in the green channel every hour for at least 16 hours with IncuCyte S3 (Essen BioScience) at 10× magnification. Nuclear-ID Red DNA stain (Enzo Life Sciences) was added after the last time point and scanned in the red channel. IncuCyte software was used to determine the total number of $YOYO^+$ cells and Nuclear-

ID^+ cells (total cells). % YOYO positive was calculated as the number of $YOYO^+$ cells divided by the total number of Nuclear-ID^+ cells.

Dextran dye (DD) release assay

BMDM stimulation was carried out as described above with the following modifications. Prior to plating, BMDMs were loaded with DD conjugates (Fluorescein isothiocyanate-dextran, 150 kDa, MilliporeSigma; Texas Red-dextran, 70 kDa, 3 kDa, ThermoFisher) using a 100 µl Neon tip (Thermo Fisher Scientific). 5.0×10^6 BMDMs were electroporated in 120 µL R buffer with 12 µl of DD at 50 mg/mL. Prior to plating, BMDMs were washed with high-glucose DMEM. Following stimulation, images of BMDMs were scanned over 16 h with IncuCyte S3 (Essen BioScience) at 10X magnification.

Sample preparation for Immunoblot

For standard immunoblot (extract only), 1.0×10^5 cells were lysed by incubation with (15~75) µl lysis buffer (10 mM Tris pH7.5, 150 mM NaCl, 1% NP-40, 2.5 mM $MgCl_2$, 0.5 mM $CaCl_2$, 5 µg/ml DNase (Qiagen), 1× Complete Protease Inhibitor (Roche Applied Science) and PhosSTOP phosphatase inhibitor (MilliporeSigma)) at 4 ℃ for 30 min. The lysate was mixed with NuPAGE LDS sample buffer 4X (Thermo Fisher Scientific) and run as whole cell lysate in SDS-PAGE or Phos-tag SDS-PAGE (FUJIFILM). For preparation of supernatant + extract, 1.0×10^6 primed BMDMs were electroporated with 1.0 µg LPS in 100 µl R buffer using Neon (Thermo Fisher Scientific) 100 µl Tip with 1,720 Voltage, 10 Width, 2 Pulse settings. Electroporated cells were added to 60 µl Opti-MEM I media to make a total of 70 µl. For nigericin stimulation, 1.0×10^6 primed BMDMs were suspended with 10 µg/ml nigericin in 70 µl Opti-MEM I media. Cells were incubated for 2 h. Samples were harvested by pelleting cells and transferring supernatant to a separate tube with 1× Complete Protease Inhibitor added to supernatant. Remaining cells were lysed in 40 µl of lysis buffer and 37 µl of LDS sample buffer 4X. Cell extracts were then combined with supernatant for immunoblotting.

RNA-sequencing

Total RNA was extracted from primed or non-primed wild-type BMDMs and *Ninj1*$^{-/-}$ BMDMs (n = 3) using an RNeasy kit (Qiagen) with on-column deoxyribonuclease digestion. Quality control

of total RNA was performed to determine sample quantity and quality. The concentration of RNA was determined using a NanoDrop 8000 (Thermo Fisher Scientific), and the integrity of the RNA was determined by Fragment Analyzer (Advanced Analytical Technologies). Total RNA (100 ng) was used as an input material for library preparation using the TruSeq Stranded Total RNA Library Prep Kit (Illumina). The sizes of the libraries were confirmed using High Sensitivity D1K screen tape (Agilent Technologies), and their concentrations were determined with a quantitative PCR–based method using a Library Quantification kit (KAPA). The libraries were multiplexed and sequenced on an Illumina HiSeq4000 (Illumina) to generate 30 million single-end, 50 bp reads. For RNA-seq analysis, the raw FASTQ reads were aligned to the mouse reference genome (GRCm38-mm10) using GSNAP (with parameters -M 2 -n 10 -B 2 -i 1 -N 1 -w 200000 -E 1 --pairmax-rna = 200000 --clip-overlap). Reads were filtered to include only the uniquely mapped reads. Differential expression analysis was performed using the voom/limma R package. Genes were considered to be differentially expressed if the $\log_2$ of the fold change was >1 or <−1 and the adjusted *P* value was <0.05.

Lipidomics analysis

5.0×10^6 primed BMDMs pellets were suspended in PBS and lysed using an ultrasound sonicator. 750 µl water, 0.9 ml dichloromethane (DCM, Honeywell Burdick & Jackson, >99.5 %) and 2 ml methanol (HPLC grade, Fisher Chemical) were added to 250 µl of cell lysate (2.5×10^6 cells) to form a single phase. After a 30 min incubation, isotopically labeled internal lipid standards (Lipidyzer™, SCIEX) were added to the mixture, followed by 0.9 ml DCM and 1 ml water. The mixture was vortexed and centrifuged at 1000x g for 10 min to achieve phase separation. The bottom layer was collected into a clean glass tube, and the upper layer was extracted once more by adding 1.8 ml of DCM. The bottom layer of the second extraction was combined with the first and dried under a gentle stream of nitrogen for subsequent LC-MS/MS analysis. Dried residue was reconstituted in 300 µl DCM:Methanol (1:1), 10 mM ammonium acetate for direct infusion and analysis on a SelexION enabled 6500+ QTRAP mass spectrometry (SCIEX) by the method previously described[38]. For cholesterol analysis, dried residue was reconstituted in 200 µl DCM: methanol (1:1). HPLC separation of cholesterol from its metabolites was performed on a reverse-phase column (Luna Omega 1.6 µm C18 100A, LC column 100 x 2.1 mm). The temperatures of the column oven and auto sampler were set at 40 °C and 15 °C, respectively. The LC flow rate was

set at 0.2 ml/min. Initial gradient conditions were 95 % mobile phase A (3:1 water : methanol) and 5 % mobile phase B (1:1 methanol : isopropanol). Mobile phase B was increased to 55 % within 2 min, further increased to 65 % over 12 min and then to 74 % in 7 min. Mobile B was held at 74 % for 11 minutes and increased to 100 % in 4 min. Mobile phase B was returned to the initial conditions within 1 min and re-equilibrated for 5 min before the next injection. The liquid chromatograph was coupled to a 6500+ QTRAP mass spectrometer operated under positive ionization mode with the following source settings: turbo-ion-spray source at 500 °C, N2 nebulization at 20 psi, N2 heater gas at 20 psi, curtain gas at 30 psi, collision-activated dissociation gas pressure was held at medium, turbo ion-spray voltage at 5500 V, declustering potential at 60 V, entrance potential at 10V and collision energy of 30 V. Sample analysis was performed in multiple reactions monitoring mode with a dwell time of 0.10 s. The transitions monitored for cholesterol and D7-cholesterol were 369.4/161 and 376.3/161, respectively. Cholesterol quantitation was achieved by creating a standard curve using 6 concentration levels of cholesterol versus its normalized response to the internal standard (D7-cholesterol).

Secretome analysis of BMDM supernatants

5.0×10^6 primed BMDMs were Neon electroporated with 5 µg of LPS with 1,720 Voltage, 10 Width, 2 Pulse settings. BMDMs were incubated in 250 µl of no FBS high-glucose DMEM for 2 h, then pelleted by spinning at 300 xg for 10 min. 20 µl of supernatants from two replicates of wild-type or *Ninj1*$^{-/-}$ BMDMs were reduced with 10 mM dithiothreitol at 60 °C followed by alkylation with 20 mM iodoacetamide at room temperature. Proteins were digested with 0.2 µg trypsin (Promega) in ammonium bicarbonate pH 8.0 at 37 °C overnight. Digestion was quenched with formic acid and the supernatants were subjected to desalting on C18 PhyTips (PhyNexus), lyophilized, reconstituted to 25 µl in 0.1 % formic acid containing 2 % acetonitrile and analyzed without further processing by reversed phase nano LC/MS/MS on a Waters NanoAcquity HPLC system (Waters) interfaced to a ThermoFisher Fusion Lumos (ThermoFisher Scientific). Peptides were loaded onto a Symmetry C18 column (1.7 mm BEH-130, 0.1 x 100 mm, Waters) and separated with a 60 min gradient from 2 % to 25 % solvent B (0.1 % formic acid, 98 % acetonitrile) at 1 µl/min flow rate. Peptides were eluted directly into the mass spectrometer with a spray voltage of 1.2 kV. Full MS data were acquired in FT for 350-1250 m/z with a 60,000-resolution. The most abundant ions found from full MS were selected for MS/MS through a 2 Da isolation window.

Acquired tandem MS spectra were searched using the Mascot (Matrix Sciences) with Trypsin enzyme specificity. Search criteria included a full MS tolerance of 50 ppm, MS/MS tolerance of 0.5 Da with oxidation (+15.9949 Da) of as variable modification and carbamidomethylation (+57.0215 Da) of cysteine as static modification. Data were searched against the mouse and contaminant subset of the Uniprot database that consists of the reverse protein sequences. Peptide assignments were first filtered to a 2 % false discovery rate (FDR) at the peptide level and subsequently to a 2 % FDR at the protein level. Label free quantification was performed using the Vista Algorithm[39] and peptide spectral matches (PSMs) per protein were visualized using Sportfire (TIBCO). Top hits were identified by multiplying the $\log_2$FC (fold change comparing *Ninj1*$^{-/-}$ to wild-type BMDMs) by the $\log_{10}$ *P*-value.

Silver staining of total proteins in culture supernatant

For visualization of secreted proteins, primed BMDMs were washed with PBS three times. Then cells were cultured in no FBS high-glucose DMEM medium for 4 h following LPS electroporation or nigericin stimulation. Culture supernatant was collected after spinning for 10 min at 300 x g. 10 µl of the supernatant were run in SDS-PAGE and proteins were silver stained by using SilverQuest (Thermo Fisher Scientific). For venetoclax and TNF+zVAD stimulation, non-primed BMDMs were cultured with venetoclax or TNF+zVAD for 16 h.

Plasmids and transient expression

cDNAs encoding N-ter FLAG (human and mouse) NINJ1, N-ter FLAG h/m NINJ2, N-ter FLAG *Drosophila melanogaster* NINJ-A, -B, -C, N-ter FLAG mNINJ1 5-Alanine-scanning mutants, N-ter FLAG mNINJ1 single Proline-scanning mutants, N-ter FLAG mNINJ1 mutants (H, K/Q mutants), and N-ter GST-FLAG mNINJ1 epitope (P_{22}-L_{31}) were synthesized and subcloned into pcDNA3.1 Zeo(+) (Thermo Fisher Scientific). For transient expression in HEK293T cells (ATCC), 2.6×10^4 cells were reverse transfected with 50 ng of plasmid with 0.16 µl Lipofectamine 2000 (Thermo Fisher Scientific) per well in 96-well plates. At 16 h after transfection, cytotoxicity was measured by CellTiter-Glo reagent.

Generation of stable cell lines

ER-Hoxb8-immortalized, wild-type and *Ninj1*$^{-/-}$ C57BL6/N mice-derived iMACs were made as previously reported[40], and maintained in RPMI 1640 medium supplemented with 10 % (v/v) low-endotoxin FBS, murine granulocyte-macrophage colony-stimulating factor (GM-CSF, 20 ng/ml, eBioscience), and 1 μM β-estradiol (MilliporeSigma). For reconstitution of *Ninj1*, cDNAs encoding non-tagged mNINJ1 or mutants ($W_{29}A$, $A_{59}P$, $K_{45}Q$) were synthesized and subcloned into the piggyBac vector (BH1.11, Genentech). *Ninj1*$^{-/-}$ iMACs were co-electroporated with NINJ1/BH1.11 and transposase vector (pBO, Transposagen Biopharmaceuticals) using Neon electroporator. Cells were selected with 6.25 μg/ml blasticidin (ThermoFisher Scientific). LPS Neon electroporation and DD release were performed as described for BMDMs above.

Blue Native (BN)-PAGE

BMDMs or iMACs were lysed with Native-PAGE lysis buffer (1 % Digitonin (ThermoFisher Scientific), 50 mM Tris pH7.5, 150 mM NaCl, 1× Complete Protease Inhibitor). After 20,800 g spin for 30 min, lysates were mixed with NativePAGE sample buffer 4X (ThermoFisher Scientific) and subjected to BN-PAGE[41] using NativePAGE 3-12 % Gel (ThermoFisher Scientific) and Coomassie G-250 (ThermoFisher Scientific).

Immunofluorescence (IF)

BMDMs were stimulated with nigericin on glass-bottom SensoPlates (Greiner). Cells were fixed with 4 % paraformaldehyde in PBS and permeabilized with 0.1 % Tween-20. Plates were blocked in PBS supplemented with 10 % goat serum and 0.1 % Tween-20 for 1 h at room temperature. Next, cells were incubated with primary antibody at 4 ℃ overnight, followed by Alexa Fluor 488 or Alexa Fluor 647 secondary (ThermoFisher Scientific) at room temperature for 1 hour. Nuclei were stained with 0.5 μg/mL HOECHST dye (ThermoFisher Scientific) for 10 min at room temperature. Primary antibodies used include: TOMM20 (clone 2F8.1, MilliporeSigma), CD44 (KM201, Abcam), and GM130 (clone 35, BD Biosciences). Plates were imaged using a 60X Plan Fluor objective on an ImageXpress Micro Confocal system (Molecular Devices). Images were subsequently processed using the scikit-image python package.

Live imaging of BMDMs

BMDMs were plated on glass-bottom SensoPlates. For LPS transfection on the glass-bottom plate, primed BMDMs were cultivated with 5 µg/ml LPS and 20 µg/ml CTB to deliver LPS inside place[37]. Where described, tetramethylrhodamine methyl ester perchlorate (TMRM, 200 µM, ThermoFisher Scientific), HOECHST, and DD-150 were used. Plates were imaged either using a 60X Plan Fluor or 20X Super Plan Fluor ELWD objective on an ImageXpress Micro Confocal system equipped with an environmental controller and gas mixer to maintain cells at 37 °C and 5 % CO_2. Images of the bright-field and transmitted light and fluorescence channels were imaged every 5 min overnight. Images were subsequently processed and videos were generated using the scikit-image python package.

Secondary structure prediction and helix modeling

Secondary structure prediction for mouse NINJ1 was performed using the JPred 4 server. Following prediction, the external alpha helical domain was modeled with SWISS-MODEL[42] and subsequently visualized with PyMOL (version 2.3.5). The structure was exported using ray-traced frames.

Conservation scores, sequence alignments, and phylogenetic tree generation

The conservation score for each amino acid residue of NINJ1 was calculated using the ConSurf[43,44] server and plotted using the Matplotlib python package. Individual ortholog NINJ1 and NINJ2 sequences obtained from the UniProt database[45] were aligned using the Clustal Omega multiple sequence alignment[46]. Phylogenetic trees were retrieved from the resulting Clustal Omega output and the alignment was visualized using ESPript 3.0[47].

***C. rodentium* infection**

12-14 week old female *Ninj1*$^{-/-}$ and littermate wild-type control mice were infected perorally with 2X10^9 CFU of log-phase cultured *C. rodentium* (ATCC 51459) after overnight fasting. Infected mice were monitored for survival for 17 days post infection.

References for method

31 Nelms, K. A. & Goodnow, C. C. Genome-wide ENU mutagenesis to reveal immune regulators. *Immunity* **15**, 409-418 (2001).

32 Kayagaki, N. *et al.* IRF2 transcriptionally induces GSDMD expression for pyroptosis. *Sci Signal* **12**, doi:10.1126/scisignal.aax4917 (2019).

33 Andrews, T. D. *et al.* Massively parallel sequencing of the mouse exome to accurately identify rare, induced mutations: an immediate source for thousands of new mouse models. *Open biology* **2**, 120061, doi:10.1098/rsob.120061 (2012).

34 Murphy, J. M. *et al.* The pseudokinase MLKL mediates necroptosis via a molecular switch mechanism. *Immunity* **39**, 443-453, doi:10.1016/j.immuni.2013.06.018 (2013).

35 Modzelewski, A. J. *et al.* Efficient mouse genome engineering by CRISPR-EZ technology. *Nat Protoc* **13**, 1253-1274, doi:10.1038/nprot.2018.012 (2018).

36 Aglietti, R. A. *et al.* GsdmD p30 elicited by caspase-11 during pyroptosis forms pores in membranes. *Proc Natl Acad Sci U S A* **113**, 7858-7863, doi:10.1073/pnas.1607769113 (2016).

37 Kayagaki, N. *et al.* Noncanonical inflammasome activation by intracellular LPS independent of TLR4. *Science* **341**, 1246-1249, doi:10.1126/science.1240248 (2013).

38 Contrepois, K. *et al.* Cross-Platform Comparison of Untargeted and Targeted Lipidomics Approaches on Aging Mouse Plasma. *Sci Rep* **8**, 17747, doi:10.1038/s41598-018-35807-4 (2018).

39 Bakalarski, C. E. *et al.* The impact of peptide abundance and dynamic range on stable-isotope-based quantitative proteomic analyses. *J Proteome Res* **7**, 4756-4765, doi:10.1021/pr800333e (2008).

40 Wang, G. G. *et al.* Quantitative production of macrophages or neutrophils ex vivo using conditional Hoxb8. *Nature methods* **3**, 287-293, doi:10.1038/nmeth865 (2006).

41 Wittig, I., Braun, H. P. & Schagger, H. Blue native PAGE. *Nat Protoc* **1**, 418-428, doi:10.1038/nprot.2006.62 (2006).

42 Waterhouse, A. *et al.* SWISS-MODEL: homology modelling of protein structures and complexes. *Nucleic Acids Res* **46**, W296-W303, doi:10.1093/nar/gky427 (2018).

43 Ashkenazy, H., Erez, E., Martz, E., Pupko, T. & Ben-Tal, N. ConSurf 2010: calculating evolutionary conservation in sequence and structure of proteins and nucleic acids. *Nucleic Acids Res* **38**, W529-533, doi:10.1093/nar/gkq399 (2010).

44 Ashkenazy, H. *et al.* ConSurf 2016: an improved methodology to estimate and visualize evolutionary conservation in macromolecules. *Nucleic Acids Res* **44**, W344-350, doi:10.1093/nar/gkw408 (2016).

45 UniProt, C. UniProt: a worldwide hub of protein knowledge. *Nucleic Acids Res* **47**, D506-D515, doi:10.1093/nar/gky1049 (2019).

46 Sievers, F. *et al.* Fast, scalable generation of high-quality protein multiple sequence alignments using Clustal Omega. *Mol Syst Biol* **7**, 539, doi:10.1038/msb.2011.75 (2011).

47 Robert, X. & Gouet, P. Deciphering key features in protein structures with the new ENDscript server. *Nucleic Acids Res* **42**, W320-324, doi:10.1093/nar/gku316 (2014).

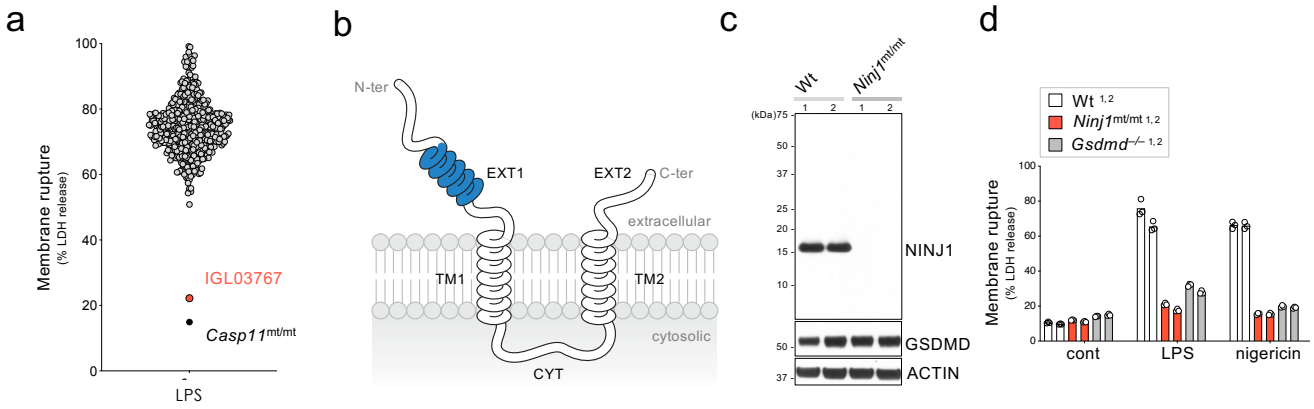

Kayagaki et al., Figure 1

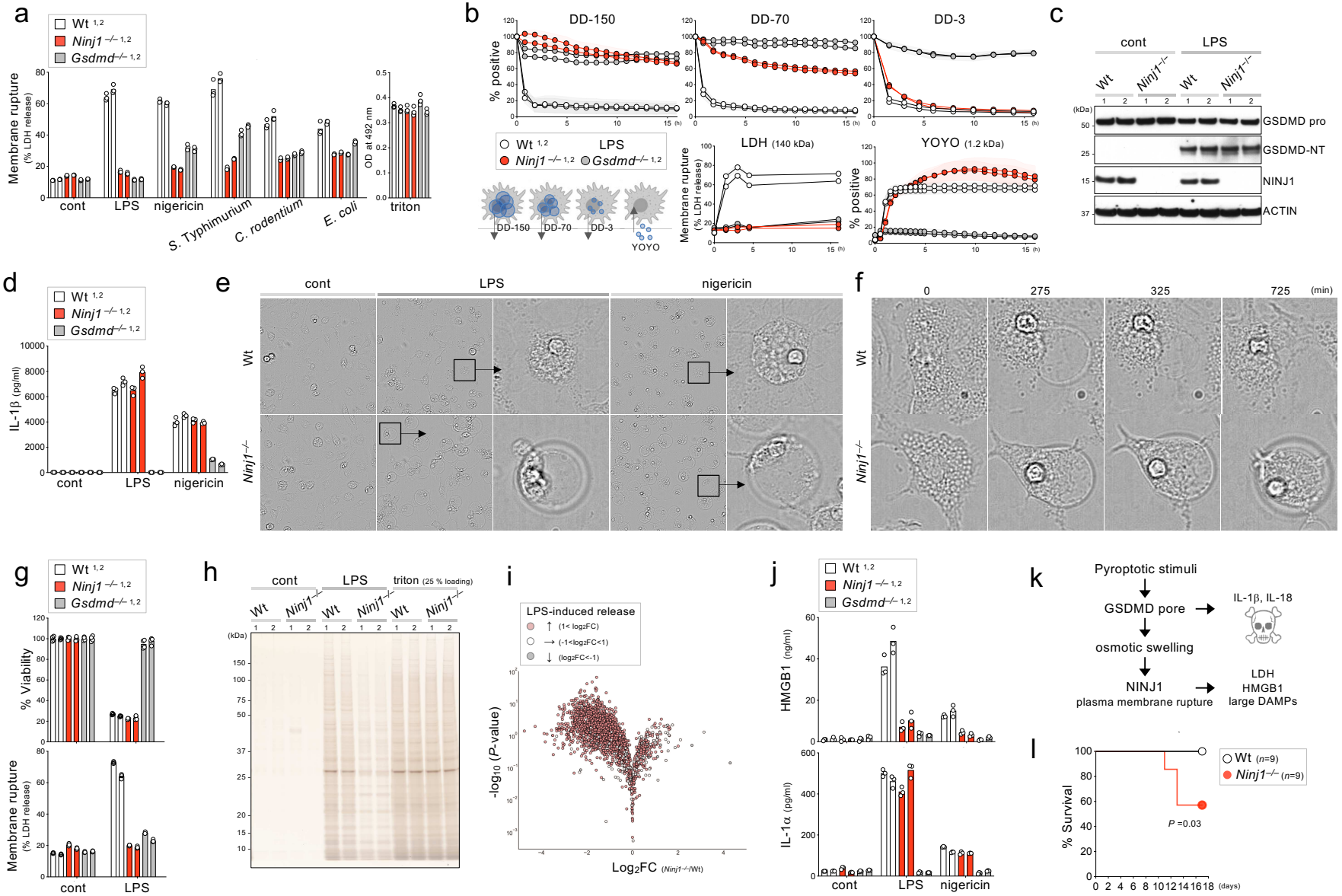

Kayagaki et al., Figure 2

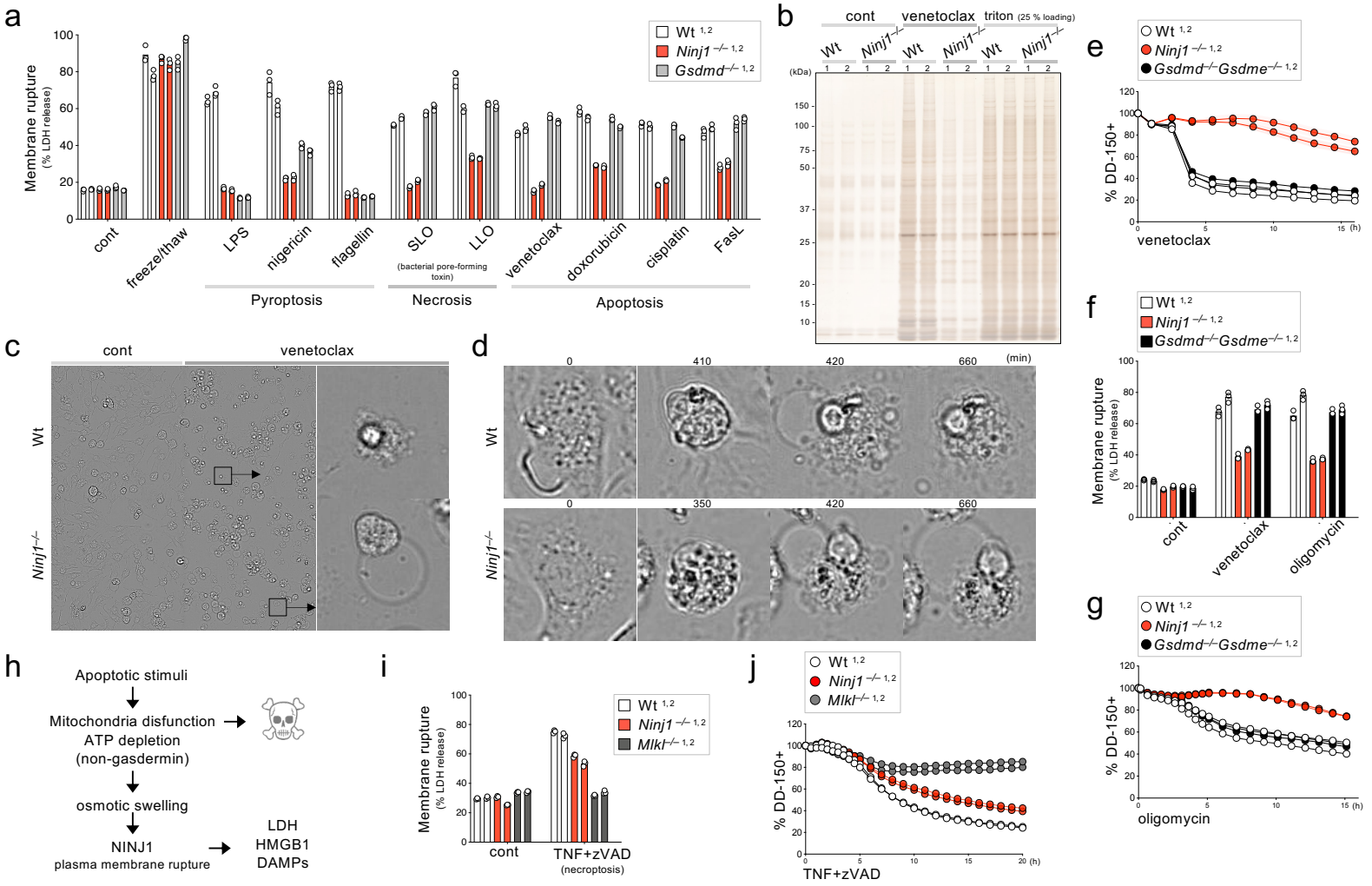

Kayagaki et al., Figure 3

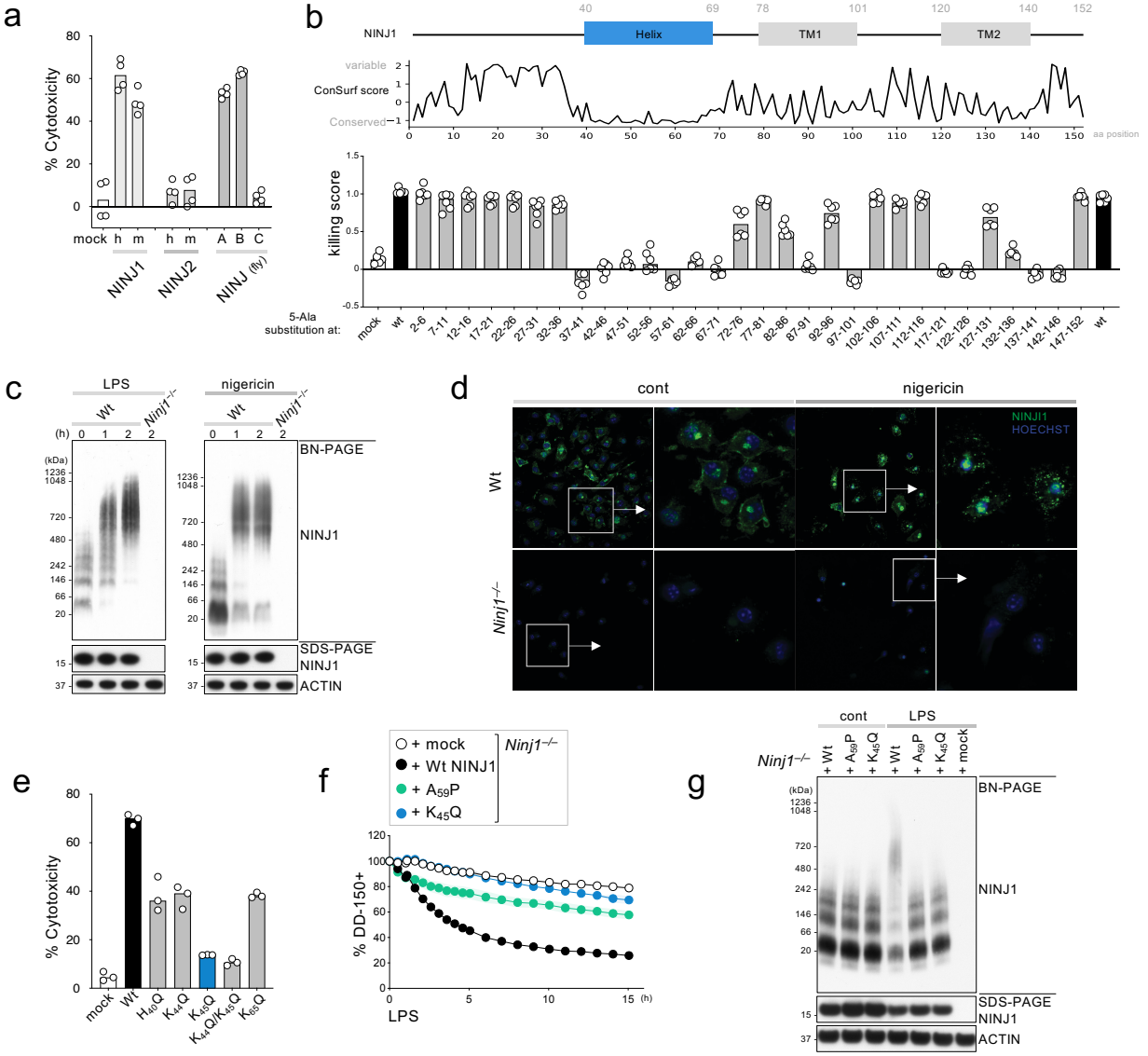

Kayagaki et al., Figure 4

a

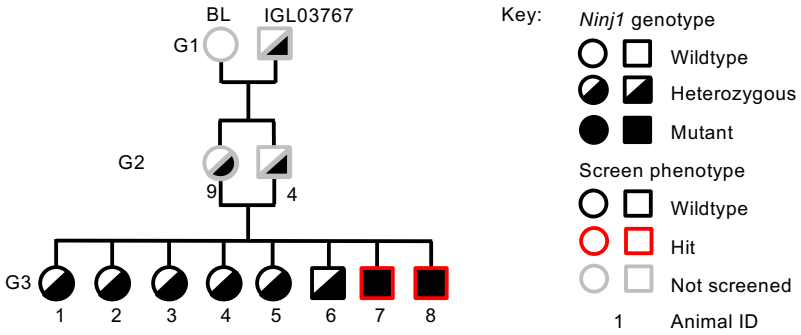

b

Chr	2	2	2	2	4	4	4	10	10	11	11	11	12	13	13	15	17	17	19
Gene	*Fcnb*	*Gm21985,Slc12a6*	*Cdan1*	*4933406J08Rik*	*Szt2*	*Ptchd2*	*Klhl17*	*Syn3,Timp3*	*Ppfia2*	*Myocd*	*Zzef1*	*Git1*	*Abcb5*	*Nid1*	*Ninj1*	*Krt84*	*Ring1*	*Mtcl1*	*Olfr1426*
Amimal																			
5	M	H	H	H	W	W	W	H	M	H	H	H	M	H	H	H	H	H	H
6	H	H	H	H	W	W	W	W	H	W	H	H	H	H	H	W	W	W	W
7	H	H	H	H	H	H	M	W	W	H	H	H	H	H	M	H	W	W	W
8	H	W	W	W	W	W	W	H	H	H	H	H	H	M	M	W	W	W	W

Key:

W	Wildtype
H	Heterozgyous
M	Mutant
	Assay hit
M	Assay hit and mutant

c

Kayagaki et al., Extended Data Figure 1

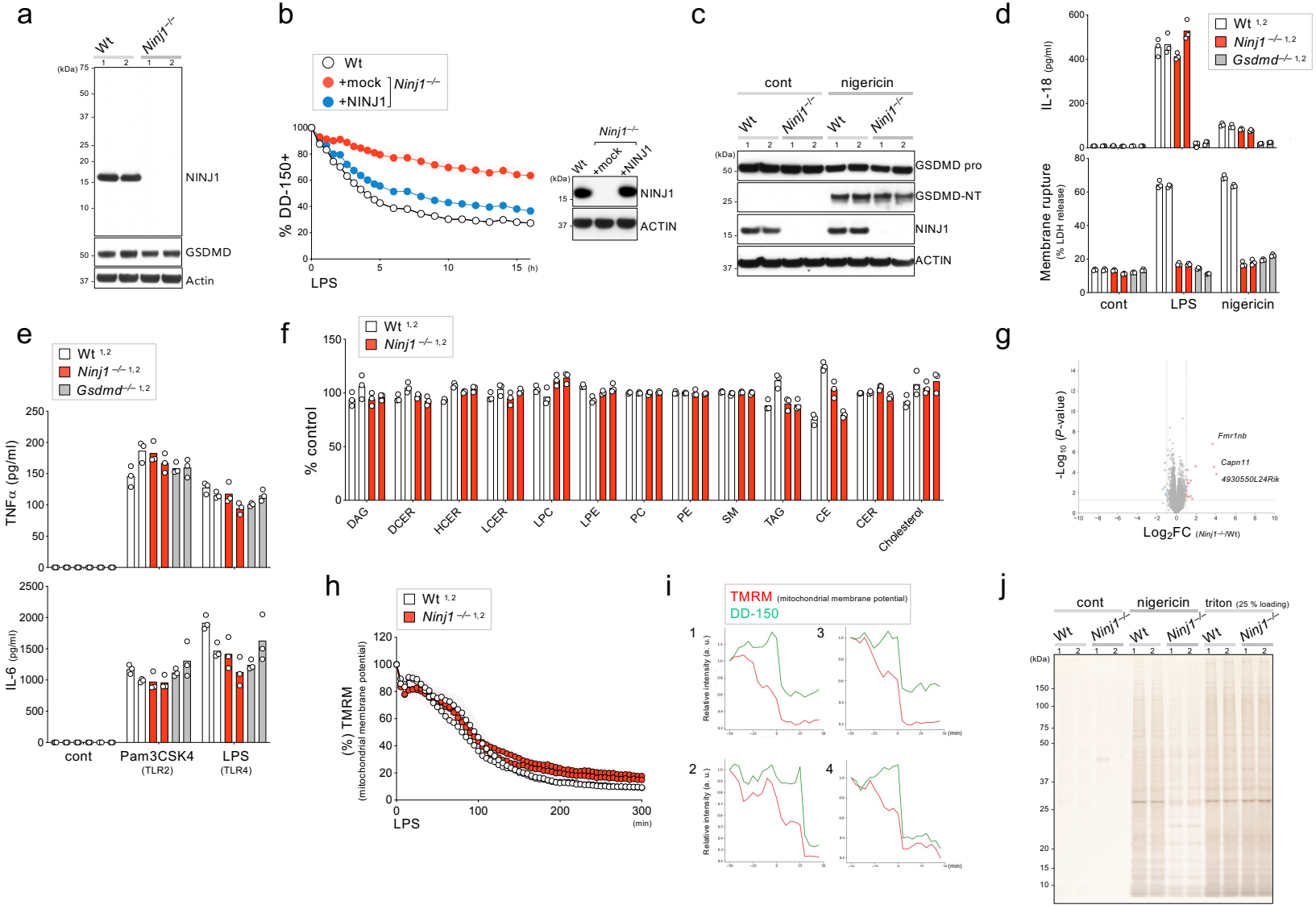

Kayagaki et al., Extended Data Figure 2

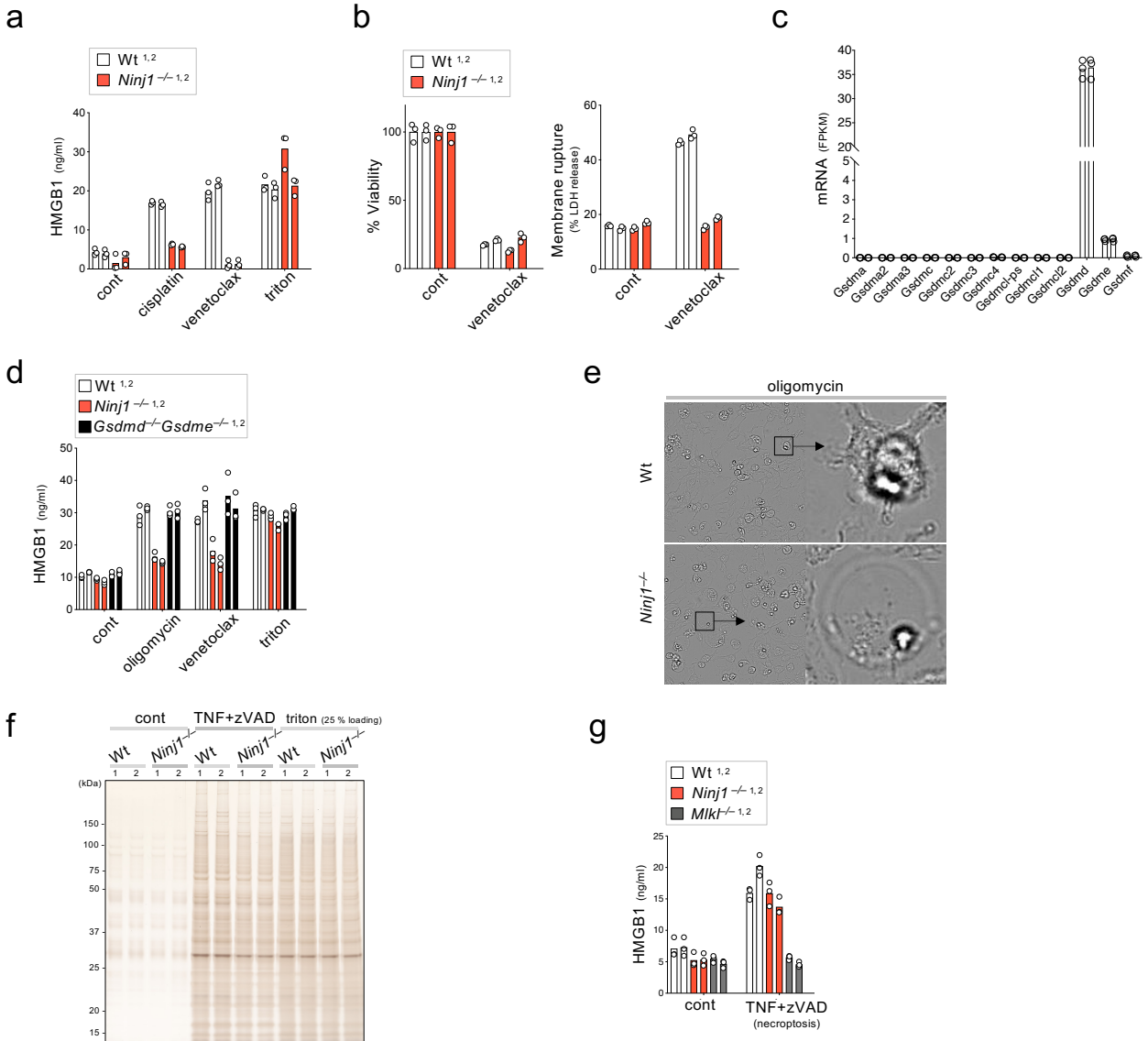

Kayagaki et al., Extended Data Figure 3

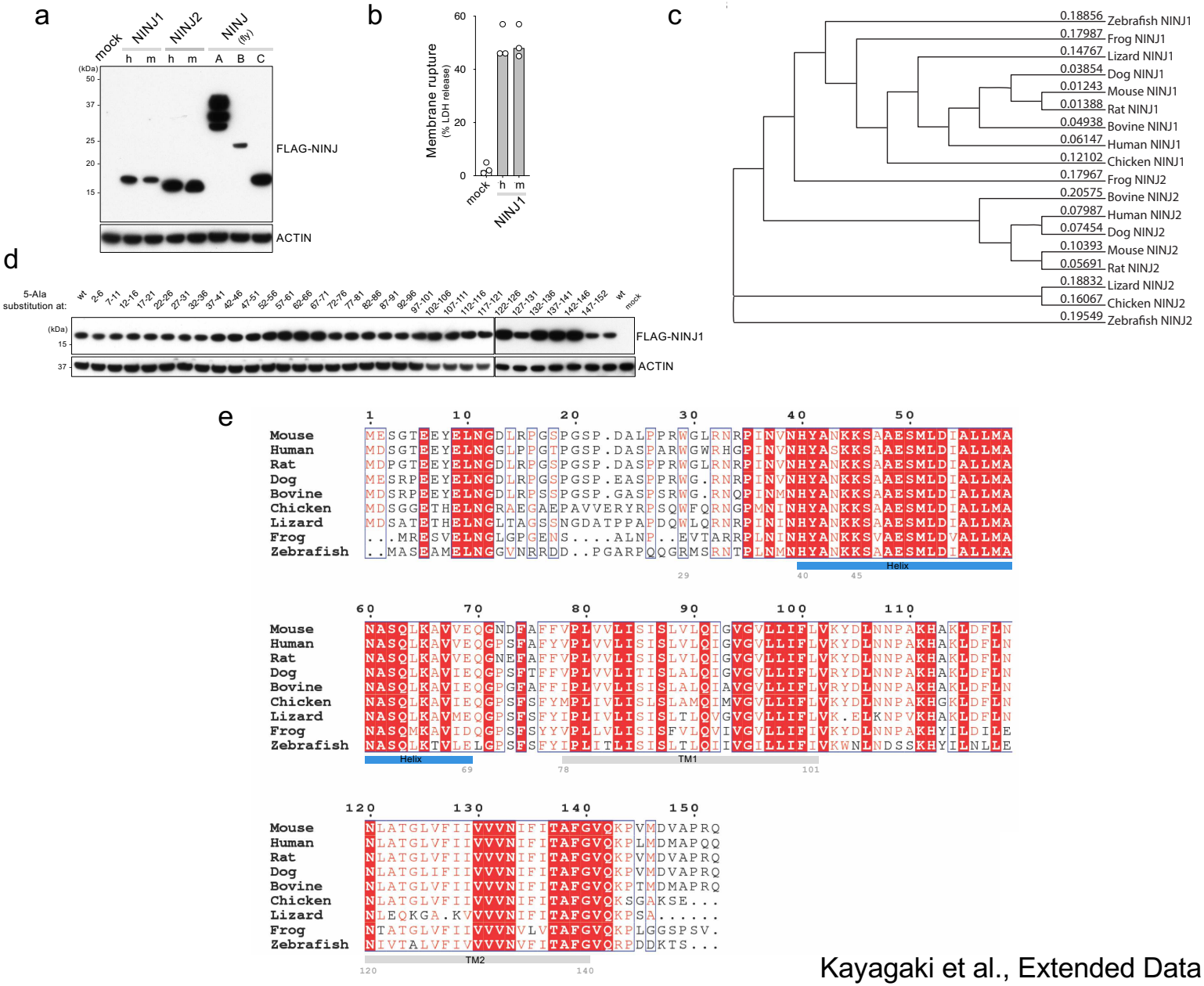

Kayagaki et al., Extended Data Figure 4

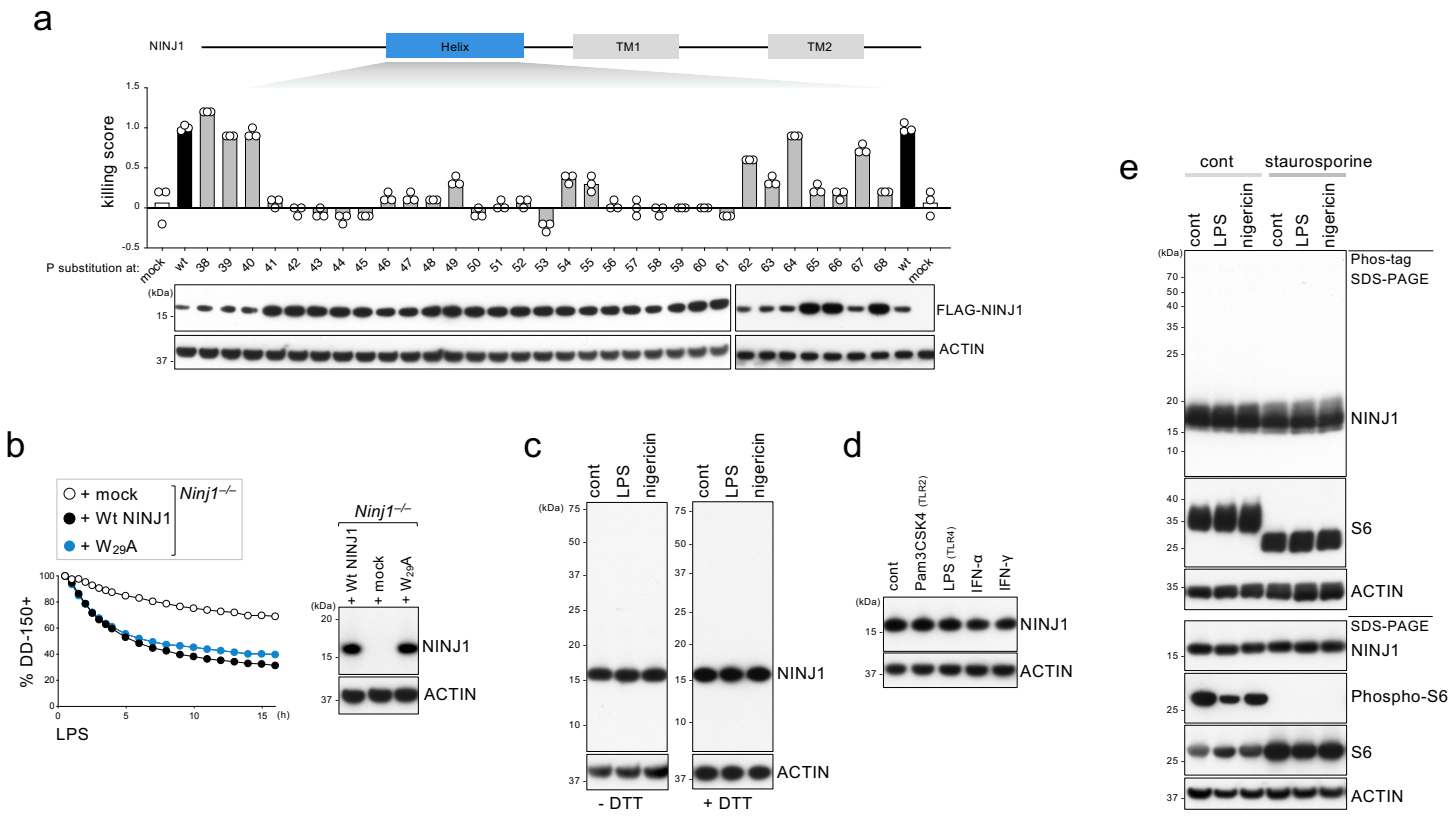

Kayagaki et al., Extended Data Figure 5

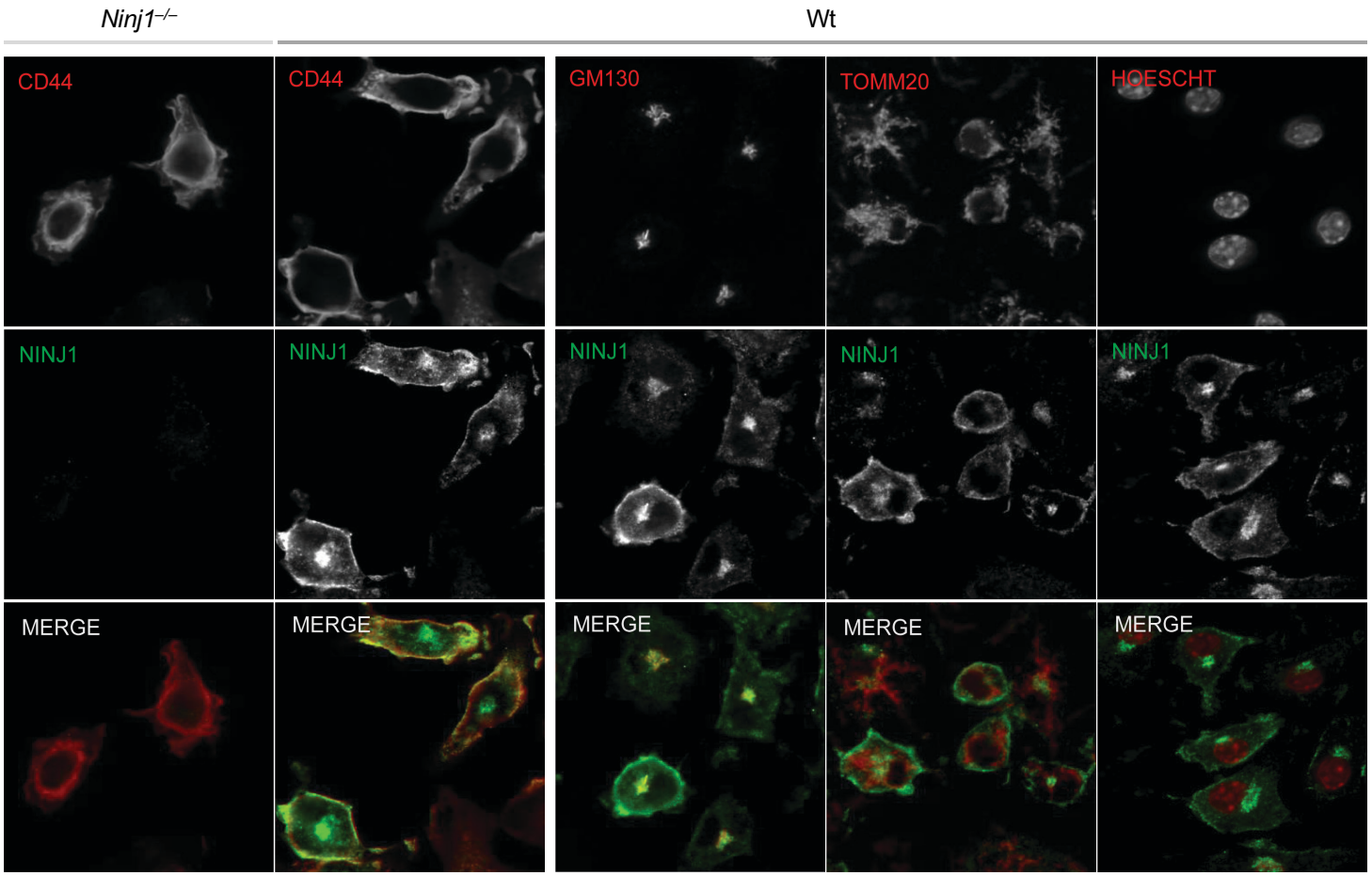

Kayagaki et al., Extended Data Figure 6

a

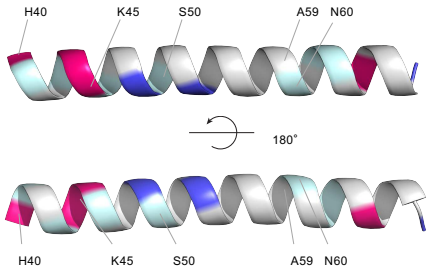

b

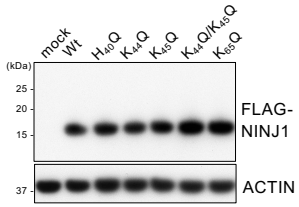

Kayagaki et al., Extended Data Figure 7

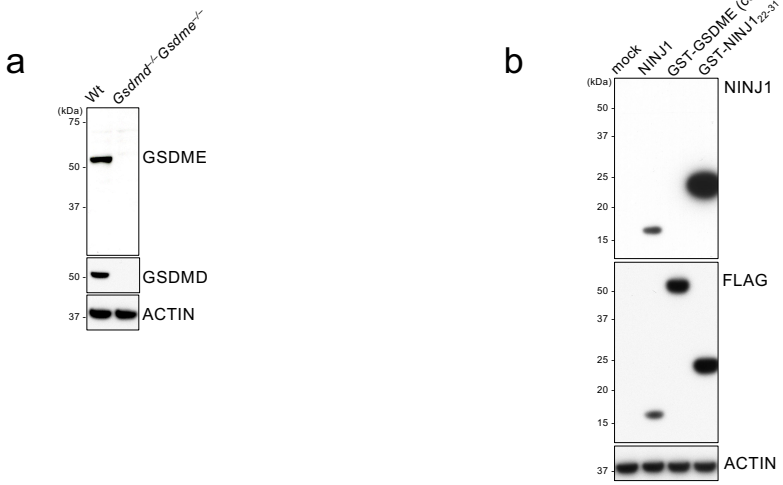

Kayagaki et al., Extended Data Figure 8

Chromosome	Coordinate (GRCm38)	Reference Base	Variant Base	Amino Acid Change	Splice Position	Polyphen Score	Polyphen Prediction	MGI Accession ID	Gene Name
2	28076801	T	C	N->S		0.68	possibly damaging	MGI:1341158	*Fcnb*
2	112351334	T	G	W->G		1	probably damaging	MGI:5439454, MGI:2135960	*Gm21985,Slc12a6*
2	120731501	T	A	M->L		0.839	possibly damaging	MGI:1916218	*Cdan1*
2	122198386	T	A	S->R		0.053	benign	MGI:1921651	*4933406J08Rik*
4	118384250	C	T	Disrupted splicing	6	N/A	N/A	MGI:3033336	*Szt2*
4	148241534	C	T	V->I		0.002	benign	MGI:2444403	*Ptchd2*
4	156233690	T	C	T->A		0.601	possibly damaging	MGI:2678948	*Klhl17*
10	86300975	G	C	Disrupted splicing	1	N/A	N/A	MGI:1351334, MGI:98754	*Syn3,Timp3*
10	106819492	A	G	T->A		0.005	benign	MGI:2443834	*Ppfia2*
11	65180944	T	C	Disrupted splicing	2	N/A	N/A	MGI:2137495	*Myocd*
11	72875126	T	A	I->N		0.001	benign	MGI:2444286	*Zzef1*
11	77505957	T	C	L->P		0	benign	MGI:1927140	*Git1*
12	118928695	T	C	D->G		0	benign	MGI:1924956	*Abcb5*
13	13476392	A	G	N->D		1	probably damaging	MGI:97342	*Nid1*
13	49193734	A	T	Disrupted splicing	2	N/A	N/A	MGI:1196617	*Ninj1*
15	101528735	T	G	D->A		0.998	probably damaging	MGI:96700	*Krt84*
17	34022575	T	C	D->G		0.093	benign	MGI:1101770	*Ring1*
17	66344319	C	T	V->I		0.001	benign	MGI:1915867	*Mtcl1*
19	12087993	A	T	D->E		0.317	benign	MGI:3031260	*Olfr1426*

Kayagaki et al., Extended Data Table 1

Gene Symbol	Description	log2_fc	adj_pval
Plec	Plectin	-1.5735411	1.34E-66
Dync1h1	Cytoplasmic dynein 1 heavy chain 1	-1.7681909	4.49E-48
Flna	Filamin-A	-1.9976335	2.96E-42
Iqgap1	Ras GTPase-activating-like protein IQGAP1	-2.263248	3.65E-27
Psmd2	26S proteasome non-ATPase regulatory subunit 2	-2.2822816	6.34E-24
Sptan1	Spectrin alpha chain, brain	-2.0996548	1.7E-25
Hsp90aa1	Heat shock protein HSP 90-alpha	-2.3249883	1.48E-22
Rrbp1	Ribosome-binding protein 1	-1.6092643	1E-31
Tln1	Talin-1	-1.6212596	9.57E-30
Rnf213	Ring finger protein 213	-1.5767322	6.98E-29
Eif3a	Eukaryotic translation initiation factor 3 subunit A	-1.5972246	9.07E-26
Diaph1	Protein diaphanous homolog 1	-2.2650811	1.06E-17
Aars	Alanyl-tRNA synthetase, cytoplasmic	-2.1223791	7.17E-18
Tcp1	T-complex protein 1 subunit alpha	-2.0447724	1.81E-18
Smc2	Structural maintenance of chromosomes protein 2	-2.5042407	1.14E-14
Ap2m1	AP-2 complex subunit mu	-2.4305962	5.72E-15
Eif5b	Eukaryotic translation initiation factor 5B	-2.0962521	3.34E-17
Smc3	Structural maintenance of chromosomes protein 3	-2.6832107	2.35E-13
Actn4	Alpha-actinin-4	-2.6133402	2.2E-13
Lmna	Prelamin-A/C	-1.7880621	5.61E-19
Snx6	Sorting nexin-6	-2.5099778	3.43E-13
Stip1	Stress-induced-phosphoprotein 1	-1.7363794	2.25E-18
Hspa4	Heat shock 70 kDa protein 4	-1.8943487	3.42E-16
Cand1	Cullin-associated NEDD8-dissociated protein 1	-2.282329	6.36E-13
Cse1l	Exportin-2	-3.0024777	5.61E-10
Sptbn1	Spectrin beta chain, brain 1	-1.8489119	2.4E-15
Lars	Leucyl-tRNA synthetase, cytoplasmic	-2.7938336	2.31E-10
Slk	STE20-like serine/threonine-protein kinase	-1.9956628	5.01E-14
Eprs	Bifunctional aminoacyl-tRNA synthetase	-2.1459888	7.87E-13
Psmd6	26S proteasome non-ATPase regulatory subunit 6	-3.2169063	9.38E-09

Kayagaki et al., Extended Data Table 2

Figures

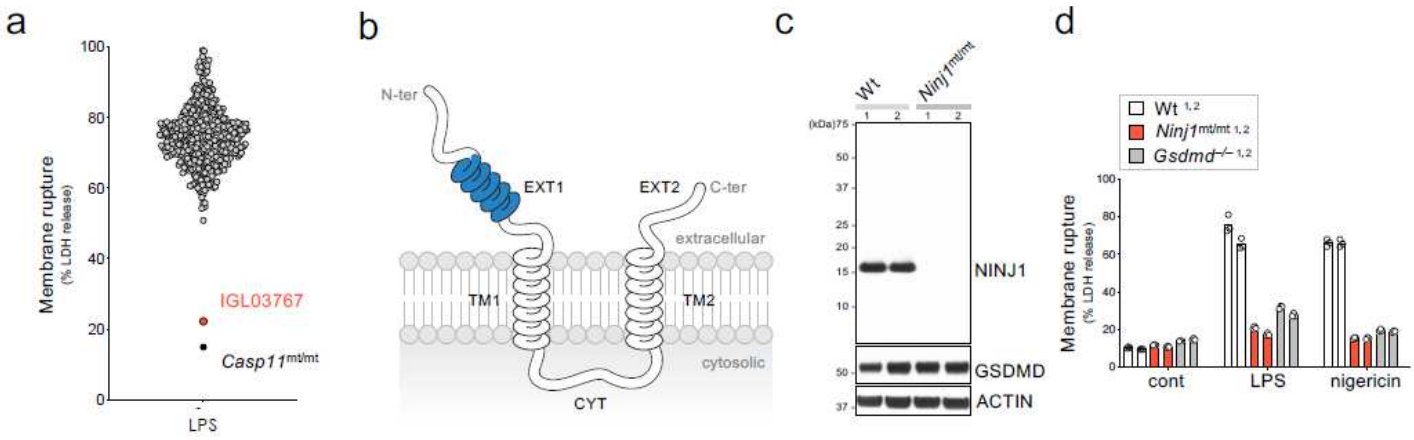

Figure 1

Forward genetic screen identifies a mutation in Ninj1 that abolishes plasma membrane rupture (PMR) a, Screening of third-generation (G3) offspring from ENU-treated C57BL/6 mice. Graph shows LDH released from Pam3CSK4 (TLR2 agonist)-primed bone marrow-derived macrophages (BMDMs) after LPS electroporation. Red dot represents IGL03767 G3 7 (Extended Data Fig. 1a, b). Grey dots represent other G3 mice in the same batch from multiple pedigrees. Black, Caspase- 11mt/mt 129X1/SvJ mouse. b, Predicted structure of NINJ1. Blue, extracellular α-helix domain. EXT, extracellular region. TM, transmembrane domain. CYT, cytoplasmic region. c, Immunoblot of NINJ1 from BMDM extracts. Lane numbers indicate different mice. n=2 per genotype. Wt, wild-type. d, LDH released from primed BMDMs stimulated with LPS electroporation or nigericin. Cont, medium alone. Data are means (bars) of at least three individual replicates (circles). n=2 per genotype.

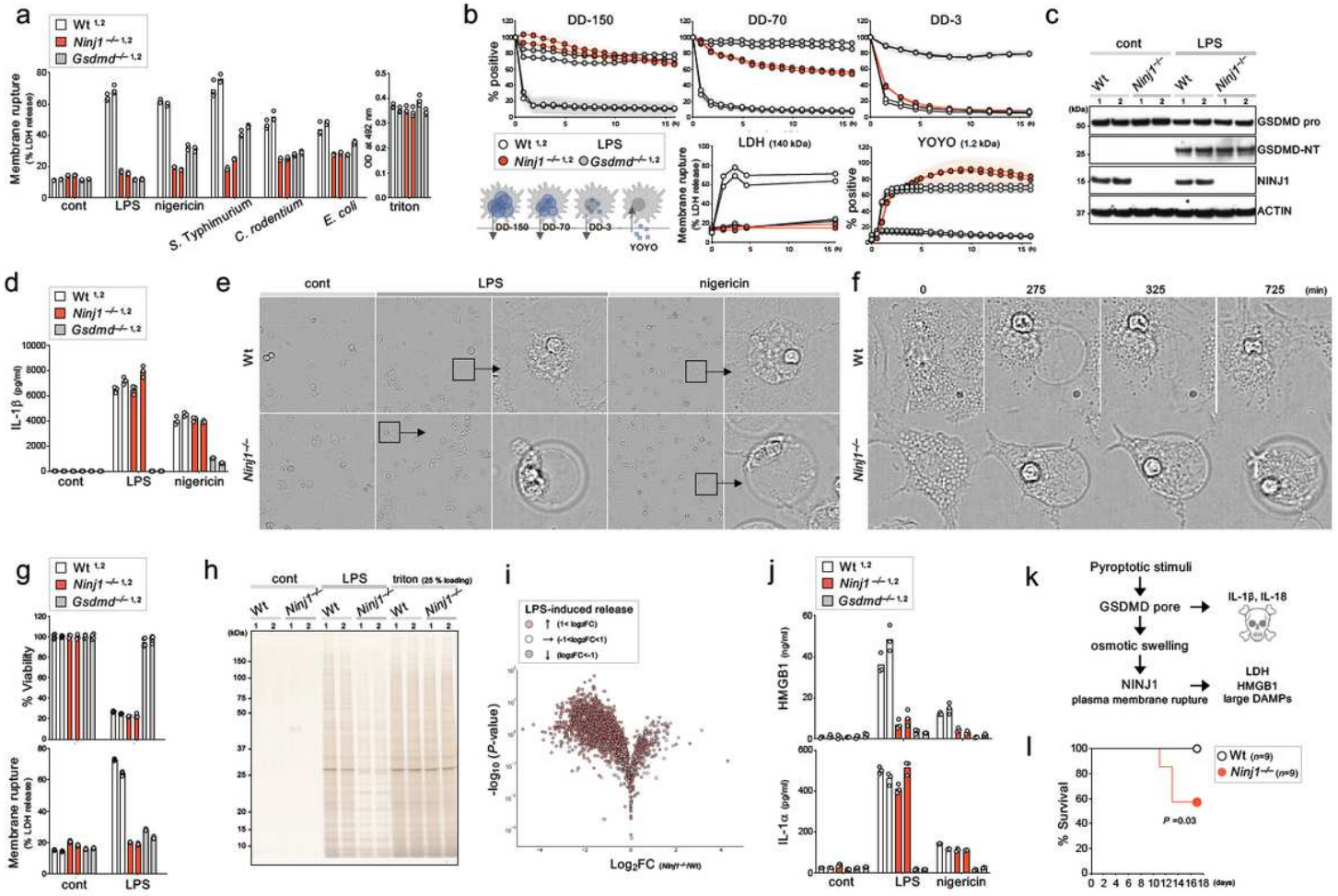

Figure 2

NINJ1 is essential for pyroptosis-related PMR a, LDH released from primed BMDMs stimulated by LPS electroporation, nigericin or indicated bacteria, or treated with 0.25 % triton. b, Release of indicated kDa sizes of dextran dye (DD) or LDH, or incorporation of YOYO-1 in live cell imaging analysis with primed BMDMs following LPS electroporation over a 16 h time course. Data are means (circles) ± SD (shaded area) of three individual replicates. c, Immunoblot of GSDMD, GSDMD-N-terminal fragment (GSDMD-NT), and NINJ1 in supernatant + extract from primed BMDMs after stimulation with LPS electroporation. d, Release of IL-1β from primed BMDMs stimulated with LPS electroporation or nigericin. e, Bright-field images of primed BMDMs stimulated with LPS transfection or nigericin for 16 h. f, Single cell time course images of primed BMDMs following LPS transfection. g, Viability (top) or LDH release (bottom) of primed BMDMs at 16 h after LPS electroporation. h, i, Silver staining (h) or volcano plot (i) of released proteins in culture supernatant of LPS electroporation-stimulated primed BMDMs. FC, fold change. j, Release of HMGB1 or IL-1α from BMDMs as d. k, Model for pyroptosis-related PMR l, Kaplan–Meier survival plots for mice infected with Citrobacter rodentium. P value was calculated by a two-sided Gehan–Breslow–Wilcoxon test.

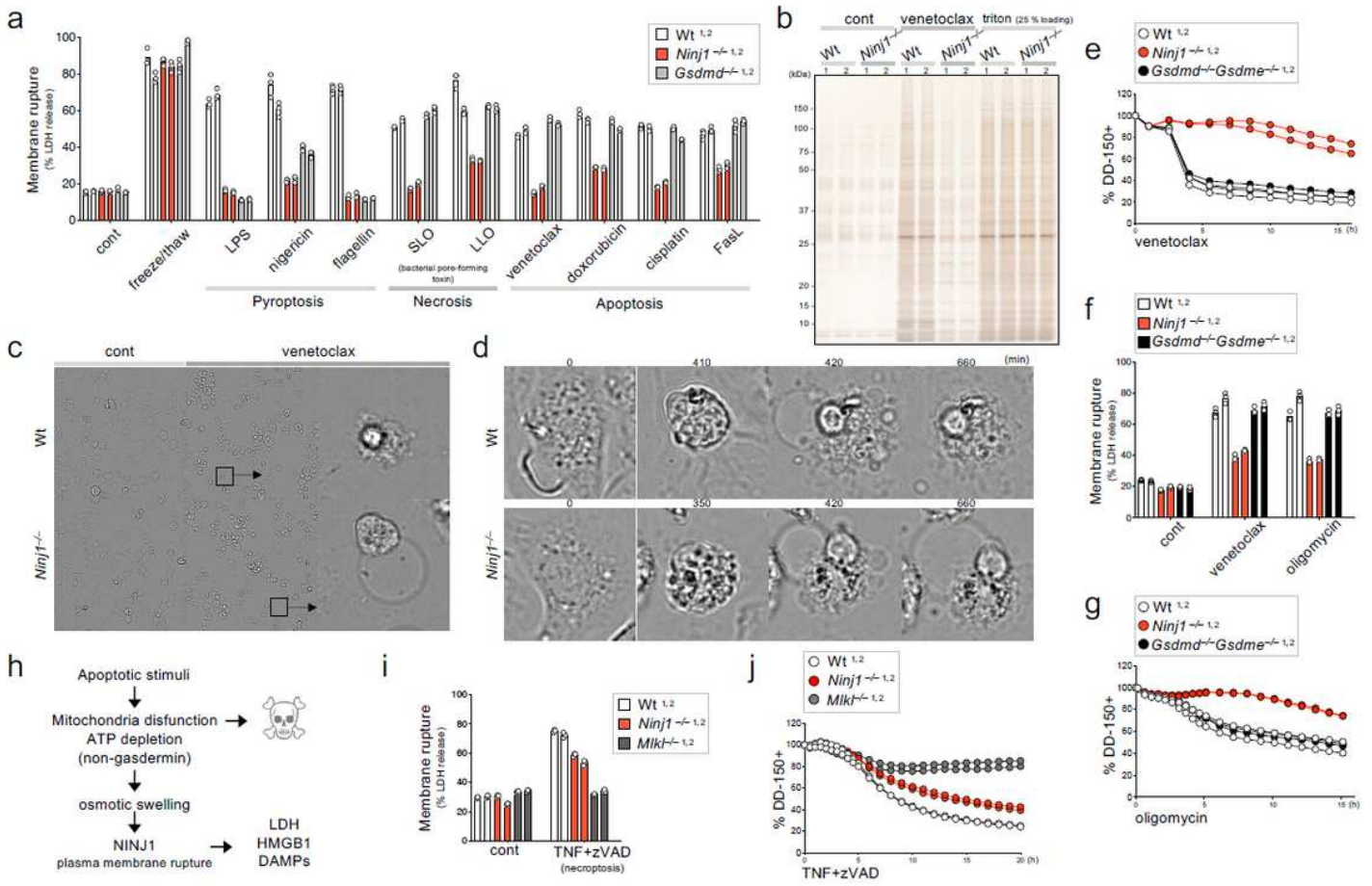

Figure 3

NINJ1 plays a global role in PMR induction a, LDH released from BMDMs after freeze/thaw cycle or culture with inducers of pyroptosis (LPS, nigericin, flagellin), necrosis (pore-forming toxins (listeriolysin O (LSO) and streptolysin O (SLO)), or apoptosis (venetoclax, doxorubicin, cisplatin and FasL). b, Silver stain of culture supernatant from venetoclax-stimulated BMDMs. c, Bright-field images of BMDMs cultured with venetoclax. d, Single cell time lapse images of BMDMs cultured with venetoclax. e, g, j, Release of DD-150 in BMDMs live cell imaging analysis following treatment with venetoclax (e), oligomycin (g), or TNF+zVAD (j). f, i, LDH release from BMDMs stimulated with venetoclax, oligomycin (f), or TNF+zVAD (i). h, Model for apoptosis-related PMR.

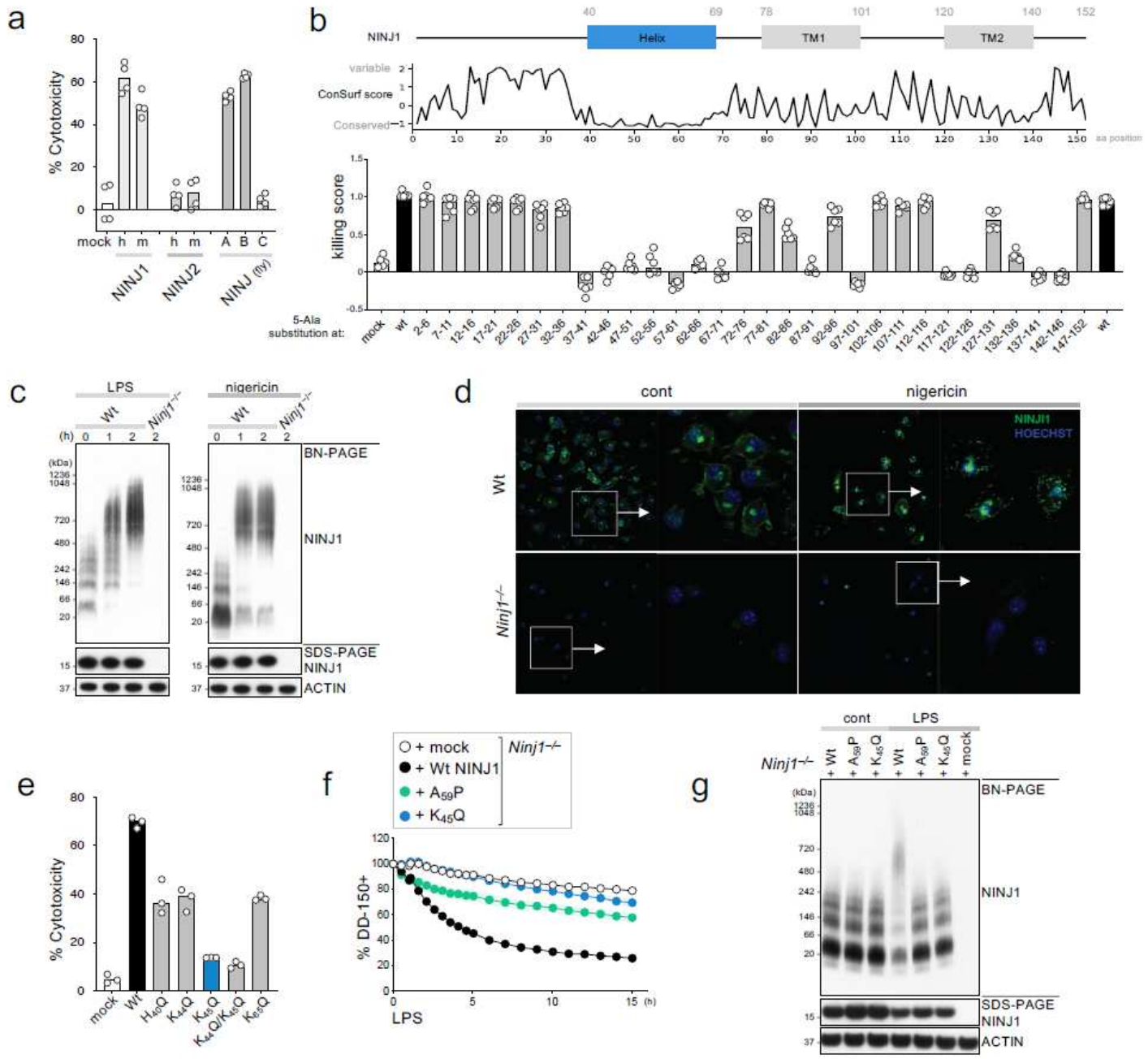

Figure 4

NINJ1 oligomerizes for induction of PMR a, Cytotoxicity of human and mouse NINJ1, NINJ2, and fly NINJ (dNINJ-A, B, C) in HEK293T cells. b, NINJ1 domain structure (top). Conservation of NINJ1 amino acid (aa) residues as scored by ConSurf profile (middle). Cytotoxicity of wild-type and 5-Ala scan NINJ1 mutants in HEK293T cells (bottom). Numbers indicate aa positions replaced by 5-Ala. Killing score is cytotoxicity normalized against wild-type NINJ1 control. c, Blue Native (BN)-PAGE analysis of NINJ1 in primed BMDMs following LPS or nigericin stimulation for indicated periods. d, Immunofluorescence microscopy of NINJ1 in nigericin-stimulated primed BMDMs. e, Cytotoxicity of NINJ1 mutants in HEK293T cells. f, DD-150 dye release from Ninj1−/− iMACs reconstituted with NINJ1 following LPS electroporation. g, BN-PAGE analysis of NINJ1 in LPS electroporation-stimulated iMACs.

Supplementary Files

This is a list of supplementary files associated with this preprint. Click to download.

- Kayagakietal.SupplementaryVideo1.pptx
- Kayagakietal.SupplementaryVideo2.pptx
- Kayagakietal.SupplementaryVideo3.pptx